Dynamic Response Localization in One-Dimensional Periodic Systems

by

Lalitha Raghavan

B.E, Osmania University, 2010

A THESIS SUBMITTED IN PARTIAL FULFILLMENT
OF THE REQUIREMENTS FOR THE DEGREE OF

Master of Applied Science

in

THE FACULTY OF GRADUATE STUDIES

(Mechanical Engineering)

The University Of British Columbia

(Vancouver)

October 2012

Abstract

This thesis contributes a novel receptance coupling technique to analyse dynamic response localization induced by bandgap mechanisms in advanced periodic light weight material and structural systems. One-dimensional structural systems are used to illustrate the technique. Localization induced by disorder and nonlinearity is investigated using numerical simulations.

The receptance coupling technique yields closed-form expressions for the location of bandgaps and their width. Numerical simulations of Blochwaves are presented for the Bragg and sub-Bragg bandgaps and compared with the bounding frequency predictions given by the receptance analysis. It is observed that the introduction of periodic local resonators narrows Bragg bandgaps above the local resonant bandgap. Introduction of two fold periodicity is shown to widen the Bragg bandgap, thus expanding the design space. Experimental measurements on a structural beam with one and two-fold periodicity are provided for validation. It is concluded that for a fixed target frequency (local resonance) of the sub-Bragg bandgap, the width can be increased by proportionally increasing the mass (and the stiffness) of the resonator. This implies that stronger coupling and heavier resonator masses yield wider sub-Bragg bandgaps. The generality of the receptance technique presented here allows straightforward extension to higher dimensional systems with multiple degrees of freedom coupling.

Insights on bandgap localization mechanisms offered by the receptance technique can be used to design periodic composite materials such as Phononic Crystals and metamaterials, and periodic structures with enhanced vibroacoustic performance characteristics.

Preface

Parts of the work presented in this dissertation are going to be published. Parts of Chapters 1, 2 and 3 will be part of the proceedings of the Materials Research Society, Fall 2012 meet to be held in November. The paper titled 'Analysis of Bandgaps in Locally Resonant Periodic Materials' will go into the proceedings. The authors of this paper are Lalitha Raghavan, Dr A. Srikantha Phani and Behrooz Yousufzadeh.

Table of Contents

List of Tables

List of Figures

Glossary

Abbreviations

FE	Finite Element
FFT	Fast Fourier Transform
FRF	Frequency Response Function
PC	Phononic Crystals

Symbols

α	Coefficient of Nonlinearity
A	Area of Unitcell of Beam
c_a	Damping Coefficient of Absorber
c_b	Damping Coefficient of Beam
C	Coupling
$\mathbf{C}$	Damping Matrix
D	Disorder
E	Young's Modulus
$\mathbf{f}$	Force Vector
γ	Localization Ratio
H	Receptance Function
k_a	Absorber Stiffness
k_r	Stiffness Ratio
$\mathbf{K}$	Stiffness Matrix
l	Unitcell Length
λ	Eigenvalues
m_a	Absorber Mass
m_b	Mass of Beam
m_r	Mass Ratio (Absorber to Beam)
M	Additional Mass
$\mathbf{M}$	Mass Matrix
ω_b	Frequency of Beam
ω_a	Frequency of Absorber (rad/sec)
ω_f	Forcing Frequency
Ω	Non-dimensional Frequency
p	Mass ratio (Additional Mass to Beam Mass)
$\mathbf{q}$	Displacement Vector
ρ	Density of Beam
θ	Angle
T	Tension
$\mathbf{T}$	Transformation Matrix

Acknowledgments

I would like to express my sincere thanks to my supervisor Dr Srikantha Phani for firstly providing me with the opportunity to pursue studies under his guidance and for his support throughout the course of my study. I would also like to thank Jess Orton and Behrooz Yousufzadeh for their help with the experiments. I extend my thanks to my colleagues and friends for healthy discussions and a congenial atmosphere for the completion of my project. Research grants from Natural Sciences and Engineering Research Council is acknowledged.

I wholeheartedly thank my parents, mother, Girija Raghavan and father, S Raghavan for their constant support not only through this work, but during every stage of my life. I also thank my brother Subramaniam Kumar for his love and encouragement. I submit this thesis at the holy feet of Jagadguru Adi Sankara.

Dedication

To My Parents

Chapter 1

Introduction

1.1 Periodic Materials and Structures

Spatially periodic micro-architectures have been used in the design of ultra-light materials (density below 10 mg/cm^3) with superior specific stiffness and strength [2] and 'metamaterials' that surpass the conventional mass-density limit of sound transmission [3]. Cellular solids based on spatially repetitive unit cells, known as lattice materials, have been developed for multifunctional applications where a mechanical function such as stiffness or strength is combined with some other property. Examples include lightweight structural applications with thermal properties or superior impact and blast resistance [4, 5]. Periodicity is also found in natural materials (the crystalline structure of solids and molecular structure of proteins), man-made structures in aerospace engineering (sandwich beams and panels with periodic core material) and biomedical devices (cardiovascular stents).

A number of periodic structures exist. Micro architecture of light weight materials such as foams, cellular or lattice materials [4–6], which exhibit superior stiffness and meta materials exhibit periodicity. Sonic or Phononic Crystals (PC) are periodic composite materials which allow for tailoring of acoustic wave propagations [7]. At a structural level, periodic structures find applications in the aerospace industry such as the ribs of the floor of an air craft [8–10], the repeating blades of a turbine [11, 12] etc. Thus the sizes of periodic structures range from a micro scale level to a structural level. Examples of periodic structures are shown in Fig 1.1.

At a microscale level, the distinction between a material and a structure cannot be made, since a structure with micro-architecture has its length scale larger than the length scale of its constituent elements.

(a) (b) (c)
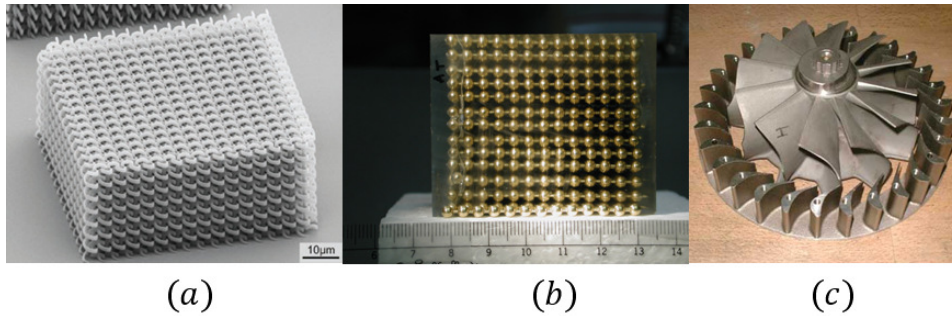
Figure 1.1: Periodic materials and structures.(a) Example of a cellular material. Structures at this length scale are often termed as materials. (b) A sonic or a Phononic Crystal (PC). (c) Periodically placed blades of a turbine.

Engineered periodic materials and structures possess inherent imperfections imposed by manufacturing constraints. Furthermore, nonlinearities arising from large deformations (geometric nonlinearity) and constitutive law of the parent material (material nonlinearity) are important considerations for engineering applications. Qualitatively new phenomena emerge when one or both conditions of linearity and periodicity are relaxed. This results in localization of macroscopic deformations or high sensitivity of the system to changes in parameters. These phenomena form the basis of investigations in this research.

1.2   Dynamic Response of Linear Periodic Structures

Periodic structures exhibit wave propagation in characteristic zones called passbands and attenuate in bandgaps, as described by Brillouin [13]. Passbands are frequency regions where the passing waves easily propagate. In the bandgaps, the waves experience exponential spatial attenuation. It is possible to vary the topology of the periodic structure to achieve desired widths of the pass and stop bands [5]. While the subject of periodic structures has been under investigation for several

years dating back to Rayleigh and several other researchers over the course of time [14–19], it is the recent development in micro-architectured materials that has once again revived interest in creating and controlling bandgaps at desired frequencies.

1.2.1 Perfectly Periodic Structures

We shall focus on the literature pertaining to developments in Phononic crystals. Phononic crystals (PC) are periodic structures made up of two materials with different elastic properties [20, 21]. Elastic wave propagation in these structures, has been under extensive study over the past few years due to the unique wave propagation characteristics that they exhibit. The pass and stop bands exhibited by PC's are a result of multiple scatterings called 'Bragg Scattering'[22, 23] and destructive interference that takes place in the structure due to periodic inclusions. The width and position of the bandgaps can be tailored by changing some of the properties of the underlying system. This property is of particular use in the control and confinement of the travelling waves [24]. Furthermore, they find applications as acoustic filters or as vibration protection devices [25].

Bandgaps relating to Bragg scattering mechanism are called Bragg-type gaps. These gaps appear around frequencies governed by the Bragg condition, $2Lsin\theta = n\lambda$, where θ is the angle of incidence and L is the lattice constant (distance between the repeating unit cells) of the periodic system and λ is the wavelength of the propagating waves.

A characteristic feature of bandgaps is that they occur at wavelengths on the order of the spatial periodicity. Since wavelength is inversely proportional to the frequency, for a given structure, it would not be possible to generate bandgaps at low frequencies. Therefore, an alternate solution is to introduce local resonators which do not require the structure sizes to be increased and at the same time yield low frequency bandgaps [3, 20, 22]. Local resonators are units with a hard core surrounded by a soft coating [26] and can be envisioned as a spring mass system. Interaction between propagating waves in a passband and local resonance of the resonator introduces a bandgap at the resonance frequency of the resonator, which are sub-frequencies of the original structure (shown in Fig 1.2) as shown in Fig 1.3. Here, a local resonant bandgap was obtained by placing periodic resonators

along a beam. A local resonant bandgap is obtained at the resonant frequency of the attached resonator. Resonant bandgaps have been observed both theoretically [27–31] and experimentally [3, 32, 33]. Liu and Hussein [34] have recently investigated the wave propagation and bandgap characteristics in Timoshenko beams to quantify the transition from a Bragg bandgap to a local resonant bandgap.
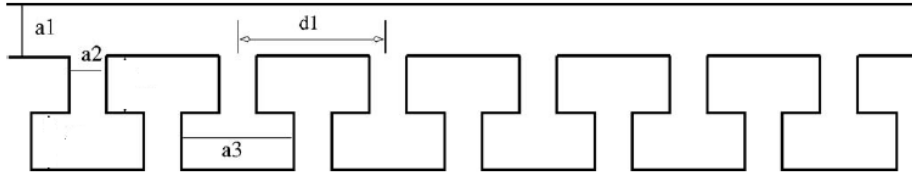
Figure 1.2: Beam with periodic resonators. The dimensions of the beam are marked herewith. Attaching resonators created a sub-Bragg bandgap.

The local resonantors are interesting not only for the sub-Bragg bandgaps that they create, but also for other interesting material property changes that the underlying system undergoes. Terms such as negative effective mass density [1, 7, 35, 36], and negative effective stiffness [36, 37] have often been used.

Consider Fig 1.4. The effective mass for this system may be written as:

$$m_{eff} = m_1 + \frac{m_2 \omega_0^2}{\omega_0^2 - \omega^2} \tag{1.1}$$

where m_{eff} is the effective mass, ω_0 is the resonant frequency of the system given by $\sqrt{\frac{k_2}{m_2}}$. When the propagating wave ω is greater than the resonant frequency of the system, the effective mass becomes negative. Thus, acceleration being opposite to the force direction, the response of the system is greatly reduced. Thus at the region of local resonance, attenuation of the waves is very high, thus creating a bandgap in that region. Similar conclusions were made in [35] where they made use of vibration theory to predict the location of the negative effective mass density. They concluded that a negative effective mass density occurs above the region of the local resonance bandgap (where $\omega > \omega_0$).
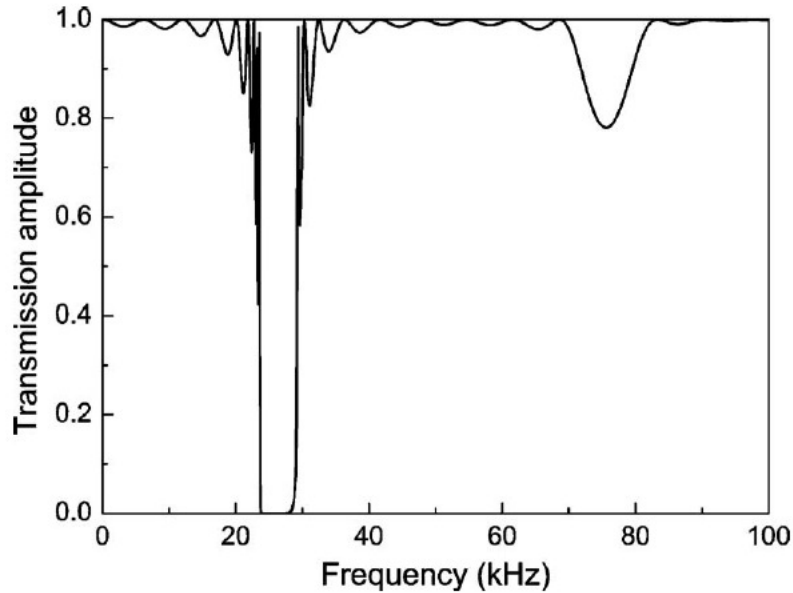
Figure 1.3: Formation of a local resonance bandgap. By attaching resonators periodically along a waveguide, a bandgap at the resonant frequency of the attached absorber is obtained.

Smith [37] considered a periodic material with two alternating layers of fluid wherein one of the fluids was assumed to have a wave speed much lower than the other. This resulted in the creation of resonance at low frequencies. It was observed that the material containing these fluids underwent a change in its effective properties such that the material's stiffness transformed from an isotropic one to an anisotropic one at the local resonance.

In many instances it becomes essential to control structural vibrations at particular frequencies. Vibration absorbers such as spring mass systems are typically used for this purpose. These absorbers are tuned so as to produce a frequency response close to zero at the excitation frequency. The idea is to attach an absorber to the main structure and force the kinetic energy of the main mass to be transferred to the absorber. The concept of local resonance is similar in the sense that the intention is to achieve zero wave propagation by introducing bandgaps at low frequencies. However, certain differences need to be noted. An absorber is attached to

5
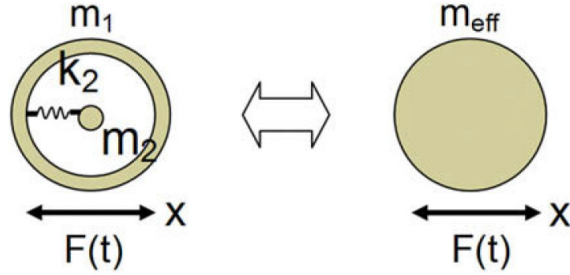
Figure 1.4: Mass in mass system and the equivalent effective mass model [1].

a mass and there is no interaction of the propagating waves to the resonant waves created by the absorber. However, a local resonator creates a bandgap at due to interaction of the propagating waves and the resonant frequencies. Additionally, changing the size of the structure does not change the region of the bandgap created by the resonators. However, an absorber is chosen depending on the size of the original structure to create an anti-resonance around particular frequencies. By adjusting the dimensions and parameters of the attached absorber, it is possible to control the size of these gaps [26] which have potential use as acoustic shields [38], tailoring waveguides [39] and silencers [40]. Hsu [22] considered stepped cylinders on PC slabs. The cylinders acted as local resonators and changing the geometry of the slab resulted in changing the width of the resonance gap. Wang et al. [27] demonstrated the effect of attaching Helmholtz resonators periodically along a waveguide, which resulted in the occurrence of a resonance bandgap. Changing the dimensions of the attached resonators and the lattice constant of the structure enabled to modify the resonant gap. Similar experiments were performed by Garcia et al. [41] wherein they obtained bandgaps at a predetermined range of frequencies by using mixed scatterers and resonators embedded in air. The work has been extended to shells [42], wherein the authors found the width of the local resonant bandgaps to once again depend on the parameter properties (mass and stiffness) of the attached resonators.

Local resonantor bandgaps corresponding to Bragg frequencies narrow in width in systems with a single type of periodicity (as will be shown in the forth-

coming chapters). However, when there is two-fold periodicity, (as in [43, 44]), with structural periodicity combining with periodic local resonators, it is possible for the existence of wide Bragg bandgaps to co-exist with the local resonant bandgaps. This property enables for tailoring the position of the Bragg bandgap such that the lowest Bragg bandgap combines with the local resonant bandgap and thereby creating a super-wide bandgap at low frequencies.

1.2.2 Disordered Periodic Structures

Engineered periodic structures inherently possess defects which arise during manufacture or during the course of their use. Periodic structures with defects or disorder in them have been known to exhibit a spatial confinement of the propagating waves, often termed as 'localization' [16, 19, 45]. Propagating waves in a periodic structure are known to reduce in transmission when they encounter disorder in the propagating medium. The mode shapes of the system become spatially-localized and display a high amplitude after which there is an exponential decay in the response as shown in Fig 1.5.

The concept of localization of propagating waves started with Anderson [46] who for the first time explained the phenomenon in the context of solid state physics. It has been conjectured that localization effects are far more general and are a generic feature of many wave bearing systems [47]. Anderson localization is a general wave phenomenon that can easily be extended to any type of waves. This phenomenon can be observed in any periodic structure that suffers from a certain level of disorder caused due to defects and/or impurities within it.

Localization as a phenomenon has the same effect as damping, the only difference being that damping reduces wave amplitudes over time, while localization confines vibrations without allowing them to propagate. This has a significant application in noise abatement. Understanding localization and the degree of disorder that will best confine propagating waves will allow for the control of noise without the use of expensive and heavy dampers. A second motivation is quite a contradiction to the first wherein one seeks to avoid this phenomenon by controlling the level of disorder in the system. Localized vibrations increase amplitudes and stresses locally and may result in severe damage. This phenomenon is mostly observed in

(a)

(b)

Exponentially decreasing
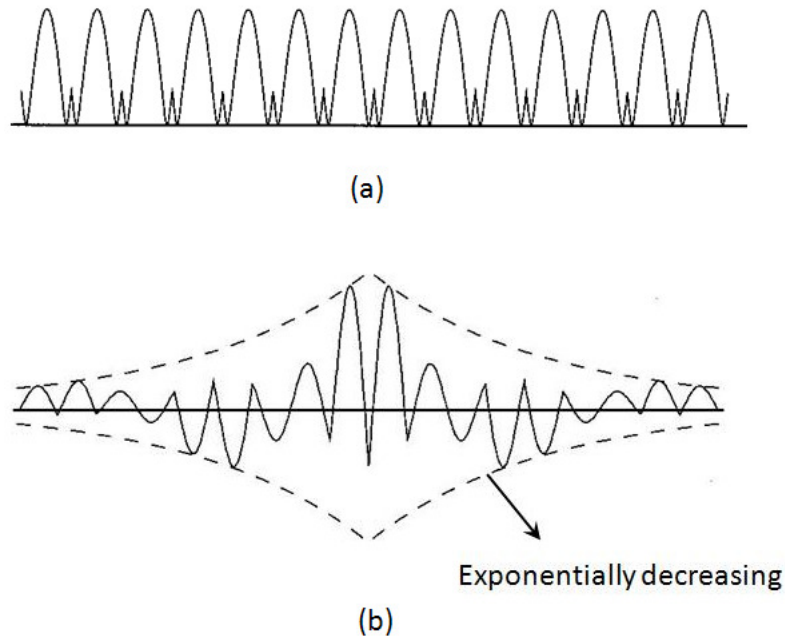
Figure 1.5: Localization within a passband. (a) Waves within the pass band of a perfect periodic structure. (b) Localized waves of a disordered periodic structure.

turbines suffering from mistuned (cracked) blades [11]. Localized vibrations increase the stresses on cracked blades and thereby damage them [12]. Thus, the understanding of the phenomenon is critical.

Localization has been observed theoretically [48, 49] in both, one and two dimensional systems at a nano-scale level. Hodges [45] in a pioneering work, examined the phenomenon in the context of structural dynamics for the first time. He considered a chain of coupled oscillators in the form of identical pendula weakly coupled to each other, as shown in Fig 1.6. Disorder was introduced in this system by varying the lengths of the pendula with respect to each other. Transmission ratios of the propagating waves for the periodic structure with and without disorder was investigated and the disordered case showed a significantly reduced transmission. The degree of localization depended greatly on the strength of disorder (W) and the strength of coupling (V). In a follow-up work, Hodges et al. [16] verified

8
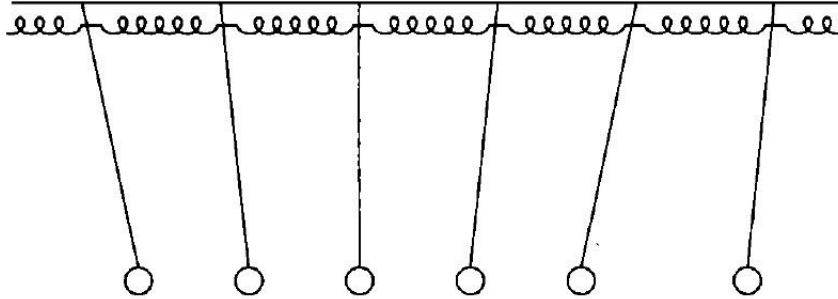
Figure 1.6: Chain of weakly coupled pendula

their theoretical findings through experiments which consisted of a string loaded with periodic beads. The bead on string model has since received a more thorough, statistical analysis [50].

It is common to consider periodic structures as simple models. For instance, coupled pendula models [16, 51, 52] and spring-mass models [53] have been extensively studied. Caruso [54] modelled a continuous bladed rotor assembly by considering it as a series of coupled pendula as shown in Fig 1.7. A complex periodic structure is represented by a simple coupled pendula model. Here, k_θ is the rotational stiffness of the springs, m is the mass of the pendula and k is the stiffness of the coupling springs. The presence of masses were incorporated using appropriate boundary conditions. Localization was observed around an imperfectly lumped mass. This type of localization is identified as a defect induced localization, where the disorder is confined to one region of the periodic structure. This differs from Anderson localization where the disorder in the system is extended throughout the structure.

Localization has also been studied in the context of eigenvalue curve veering. Nearly identical coupled oscillators demonstrate a repulsion in their natural frequencies when a parameter in the system is changed. The region of repulsion termed as 'veering' is a region of high sensitivity. This has found applications in micro sensing devices to detect small changes in the system (disorder) by observing the behaviour of the natural frequencies [55]. Pierre[52] observed the phenomenon of eigenvalue loci veering when he considered weakly coupled identical pendula
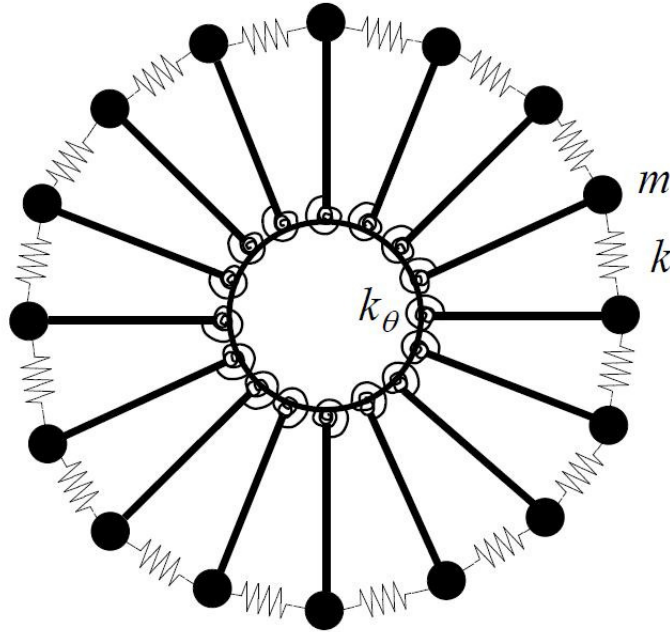
Figure 1.7: A models of bladed rotor assembly.

with a small level of disorder and concluded that eigenvalue loci veering and mode localization were indeed different manifestations of the same phenomenon. Several studies were pursued thereafter to investigate veering in the light of localization, which will be presented in greater detail in Chapter 4.

While the effect of disorder is extended throughout the structure, localization needs to be studied from a statistical view point in order to quantify the degree of localization. Pierre [56] conducted statistical investigations to study weak and strong localizations. Earlier, Hodges [16] had used the statistical perturbation methods to detect the degree of localization. These studies were confined to one-dimensional systems. Studies have since extended to two dimensional systems as well [57, 58].

1.3 Dynamic Response of Nonlinear Periodic Structures

Nonlinearities may be geometric or material in nature as has been mentioned in Section 1.1. Nonlinear wave propagation in periodic structures was first investigated in solid-state physics wherein researchers were trying to identify the effects of the nonlinear Schroedinger wave equation as the waves passed through periodic electrons. Maynard [8] conducted experiments for the first time at a macroscopic scale to determine the effects of nonlinearity on localization. His experiment consisted of a steel wire with periodically arranged masses as shown in Fig 1.8. An actuator which was free to move along the length of the steel wire induced transverse vibrations on the wire. A horseshoe magnet placed at the opposite end recorded the transmitted waves. For increased drive amplitudes (higher nonlinearities), Maynard's experiments showed that the localization effect weakened, but the weakening in localization was not consistent with increasing drive amplitudes. The reasons for the fluctuations in the observed data were not reported. In other words, the experiment was inconclusive in proving the effects of nonlinearity on Anderson localization. On the other hand, a contrasting conclusion was made by Richoux et al. [59] who considered a one dimensional string loaded with periodic masses. They concluded that localization increases in the presence of disorder and nonlinearity. However, the systems considered in the above two cases differ in the nonlinearities. In Maynard's experiments, the string possessed nonlinearities extended over a range of unit cells, while in Richoux et al.'s experiment, the nonlinearities were restricted to a particular site.

Comprehensive literature on nonlinear wave propagation in periodic structures exists in the field of solitons [60, 61]. Light wave propagation in periodic wave guides under nonlinearity has been explored by several researchers. Bradley conducted studies on wave propagation in periodic waveguides in linear and nonlinear regimes [62–64]. He developed a theory for nonlinear wave propagation under strong dispersion. He concluded that the result of a nonlinear medium is the generation of a backward travelling secondary wave which inhibits propagation of the wave and thus reduces transmission.

Small nonlinearities may be considered as a disorder and/or defect as they tend to break the symmetry of a periodic structure. Energy can become localized at a
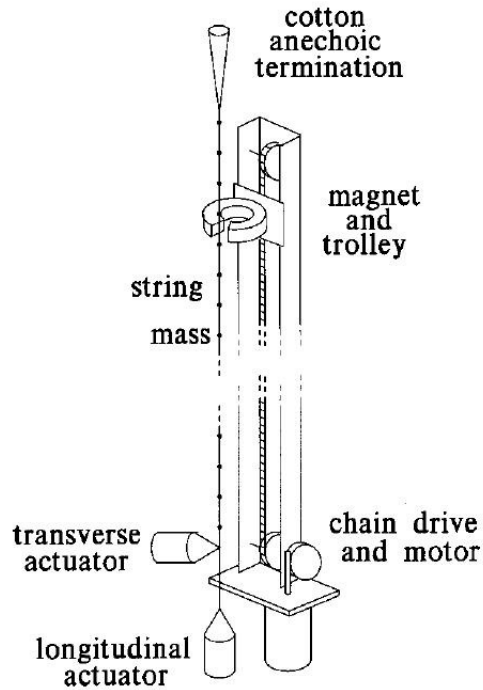
Figure 1.8: One dimensional acoustic Anderson localization experiment

specific location in a discrete system as a result of the nonlinearity of the system and not due to any defects or impurities within the considered systems [65]. Time periodic, spatially localized, stable solutions called 'breathers' can exist in non-linear periodic structures and have been under extensive study for over a decade. Aubry and MacKay [66] rigorously proved the existence of breathers in nonlinear disordered chains.

Nonlinear systems with disorder can prove useful for energy transfer [67]. This means that unnecessary vibrations in a periodic structure could be transferred to a single nonlinear attachment sink. Recently, forced response on coupled disordered pendula has been studied by Tjavaras et al. [51] with interesting results. They concluded that weak nonlinearities promote localization, while stronger nonlinearities weaken localization. Their results though unique, were not investigated thoroughly

and the anomalies observed for varying levels of nonlinearity with regards to the localization were not addressed.

1.4 Summary and Discussion

Periodic structures offer a wide range of subjects for investigating wave propagating characteristics. From the literature survey, it is evident that there is significant scope in tailoring the local resonant bandgaps in perfect periodic structures. However, there does not exist a very clear understanding of the bandgap formation. Also, the available analytical approaches for predicting the widths of the bandgaps often make use of transfer matrix methods [68] or seek to solve the underlying partial differential equations. There is a simple analytical approach lacking in the analysis of bandgap formation. Thus, there is a need to investigate local resonance bandgaps in further detail.

Secondly, it has been identified that disorder induces a confinement of propagating waves in periodic structures. Disorder, coupling and nonlinearity are some of the factors that mainly influence localization. It may be seen that the effect of nonlinearity on localization is still a vastly debated subject with the type of nonlinearity, the effect of damping, the strength of nonlinearity and nonlinearities coupled with disorders being factors which could highly influence the effect of nonlinearity on localization.

1.5 Scope and Outline

The objective of this thesis is to develop a better understanding of the phenomenon of wave propagation in periodic structures. Two broad objectives may be outlined as an outcome of the literature survey. There is a need to develop analytical methods to predict the occurrence and to control the widths of bandgaps of locally resonant periodic structures, which finds applications in vast number of areas as has been mentioned explicitly in Section 1.2.1. The second objective of this work is to study the influence of weak nonlinearities on localization in a two degree of freedom system with a view to extend to periodic systems in future.

A general understanding of bandgap formation is first presented in Chapter 2. Thereafter, unit cell analysis using Bloch's theorem will be demonstrated. Ana-

lytical techniques using *Receptance* formulae to predict the widths of local resonant bandgaps for periodic second and fourth order systems with attached local resonators is also presented as part of the chapter. The work will help designers choose optimum parameters of the resonators in order to achieve the widest possible local bandgap. The influence of one and two-fold periodicity on the local resonant and Bragg bandgaps will also be shown. Additionally, the extraction of damped dispersion curves and the effect of damping on the width of the bandgaps will be reported.

We present experimental results verifying our theoretical predictions of Chapter 2 as part of Chapter 3. The experiments include tests on a fixed beam with various types of periodicity and their effects on the bandgaps.

Chapter 4 presents an extensive analysis of coupled oscillators to understand the behaviour of localization under a harmonic force under the influence of linearity and small nonlinearity. A two degree of freedom spring-mass system will be analysed for the influence of nonlinearities. One term harmonic balance on the governing equations is performed to predict the regions of localization and delocalization on the response. The influence of various parameters on localization will additionally be presented. Concluding remarks, limitations of the current work and scope for future areas of research are identified as part of Chapter 5.

Chapter 2

Analysis of Localization Through Bandgap Mechanisms

2.1 Introduction

The propagation of waves in periodic structures is an area of great interest in applied physics, materials and engineering community worldwide. As mentioned in the previous chapter, periodic structures exhibit pass and stop bands, corresponding to regions where propagation of waves can and cannot take place respectively, due to Bragg scattering. These gaps are also influenced by various types of periodicity [34]. In order to create bandgaps at the sub-Bragg frequencies, periodic structures such as phononic crystals often employ the use of periodically placed resonators in order to create a bandgap at the resonant frequency of the attached resonator, which lies in sub-Bragg frequency regime. Previous analysis by Mead [17] and recently by Mace et al. [68] predict the bounding frequencies of the bandgaps and have likened them to the natural frequencies of the unitcell with different end conditions. The authors have considered a string with periodic resonators and used a transfer-matrix method to obtain the bounding frequencies of the attenuation zones. Although this analysis has proved to be very useful and insightful, there is still a need to understand the formation of these bandgaps in greater detail in order to make full use of the properties that they exhibit for vibration isolation [69], shielding [38] etc. The aim of this chapter is to develop a general understanding of

bandgap formation and to provide simple analytic techniques which could characterise the widths of the bandgaps.

Here, we build on earlier work in periodic structures [17, 19], but follow a different approach of receptance coupling to predict the bounding frequencies of a resonant bandgap. Design guidelines for local resonators can be readily obtained from the table of receptance functions [70]. The mechanism of bandgap formation is first presented in Section 2.2. Floquet-Bloch [6, 13] theorem and associated properties of periodic structures are then presented in Section 2.3. This enables us to investigate the characteristics of an infinitely repeating periodic unitcell. Wave propagation analysis is presented on the basis of the Floquet-Bloch theorem. In Section 2.4, we introduce the concept of local resonance by attaching locally resonant oscillators (spring mass dampers) to a continuous system. The analysis is first performed on a second order system (where the governing differential equation contains a second-order derivative with respect to the spatial variable) such as a string with attached resonators using Receptance coupling technique. Thereafter, we extend the same to a fourth order system (where the governing differential equation contains a fourth-order derivative with respect to the spatial variable) such as a Timoshenko beam. Analysis of various types of periodicity on a beam is presented in Section 2.5. The effect of various parameters on the width of the local resonant bandgap will additionally be presented. The extraction of damped dispersion curves and the effect of damping on the width of the bandgap is presented in Section 2.6. Finally, a summary of our findings is reported in Section 2.7.

2.2 Mechanism of Bandgaps

Before we attempt to replicate the wave propagation characteristics in a linear system, it is worthwhile to understand some of the basic underlying concepts and terms to be used in this chapter.

A continuous periodic structure has an infinite number of alternating attenuation zones and propagation zones [19]. It has been established [18] that for a symmetric unitcell the edges of the bandgap are bound by the so called 'locked' or 'fixed' and 'free' *natural* resonant frequencies of the unitcell. Here, symmetric unitcell is defined to be the the one with a reflective symmetry about its mid-plane

so that the left and right edges are indistinguishable. For asymmetric unitcells it is not guaranteed that the band edges are bound by the resonant frequencies of the unitcells. Here we focus only on material and structural systems with a symmetric unitcell.

In order to investigate the properties of an infinite, symmetric system, Bloch's analysis [6, 13] employs the properties of the unitcell of the system to predict the response of the entire system. Thus, analyzing the band structure of a unitcell will provide information about the wave propagating in the entire periodic structure. This shall be shown in the following section. However, within the unitcell, the propagation of the wave is quasi-periodic (between the irreducible non-dimensional wavenumber region of 0 to π) [71]. This would imply that the group velocities at the ends (non-dimensional wavenumbers at $k = 0; k = \pi$) be zero for quasi-periodic boundary conditions to be satisfied. A solution that is odd or even in the unitcell is chosen for convenience. This implies that either the displacements at the two ends be zero or, conversely, the rotations at the two ends be zero. This is satisfied by considering either simply supported ends or guided ends for the unitcell. The simply supported end condition yields only rotational motion at its two ends (considering that there is no axial motion), while the guided end condition yields only vertical displacements at its two ends. This would mean that quasi-periodic boundary conditions are satisfied and thereby yield the bounding frequencies of the attenuating zone. A fixed end condition would not satisfy the even or odd function condition and hence cannot be used to predict the bounding frequencies.

Mead [17] has shown mathematically that for a propagating free wave through a periodic, symmetric system, the bounding frequencies of the attenuating zone are characterized by $\cosh(kx) = \pm 1$; where kx is the propagating constant. It has been formally proved therein that the simply supported and guided end conditions for the unitcell satisfy this condition and agree with the equation for the bounding frequencies, provided the unitcell is perfectly symmetric. On considering a symmetric unitcell, it is required that their modes are symmetric or anti-symmetric. Symmetric modes require that the bounding frequencies have same sign of displacement at their ends or opposite signs for the rotations. Similarly, anti-symmetric modes require that the displacements at their ends have the opposite signs and the rotations

17

have the same sign. The boundary conditions that satisfy these conditions would be simply supported and guided. As mentioned above, a fixed boundary condition for instance would not satisfy the above properties, as it offers no flexibility in displacement and rotation, as it is required that there is a continuous wave propagation between the unitcells. Once the displacements and the rotations are locked, the boundaries would no longer satisfy the quasi-periodic condition.

Fig 2.1 shows the three cases for a beam with periodically placed masses, periodically placed resonators and a beam with two-fold periodicity. We consider the unitcells of these systems to explain the bandgap formation in them.

It is well known that the natural frequencies of a simply supported uniform beam and guided uniform beam are identical, except for a zero frequency rigid body mode present in the guided beam [70]. Thus for a beam with no inclusions, we expect no bandgaps as seen in Fig 2.2(a).

To understand the bandgap formation in a beam with periodic masses, consider the natural frequencies of the unitcell with a mass placed at its mid span. The principal modes of a simply supported beam are sine curves, while those of guided beams are cosine curves [70]. Thus, the odd modes of the guided beam are uninfluenced by addition of periodicity (due to coincidence of the periodicity with the node position) and similarly, the even modes of the simply supported beam are uninfluenced by the periodicity. This results in the separation of the edges and consequently the formation of bandgaps as shown in Fig 2.2(b). The width of the bandgap is the difference between the natural frequencies of the unitcell in the two boundary conditions. Thus the first bandgap width is the difference between the first natural frequency of the simply supported beam and the second natural frequency of the guided beam. A schematic showing the bandgap formation along with the mode shapes of the unitcells is shown in Fig 2.3

A similar analysis explains the appearance of a bandgap due to a periodic local resonator. By replacing the periodic masses with periodic resonators, the coupling between the rigid mode of the guided beam and the resonator leads to two frequencies. The first is a zero frequency rigid mode and the second is a finite frequency mode whose value depends on the properties of the resonator. With increasing stiffness of the resonator, this frequency now increases, causing the formation of a local resonant bandgap. However, now the even modes associated with the guided
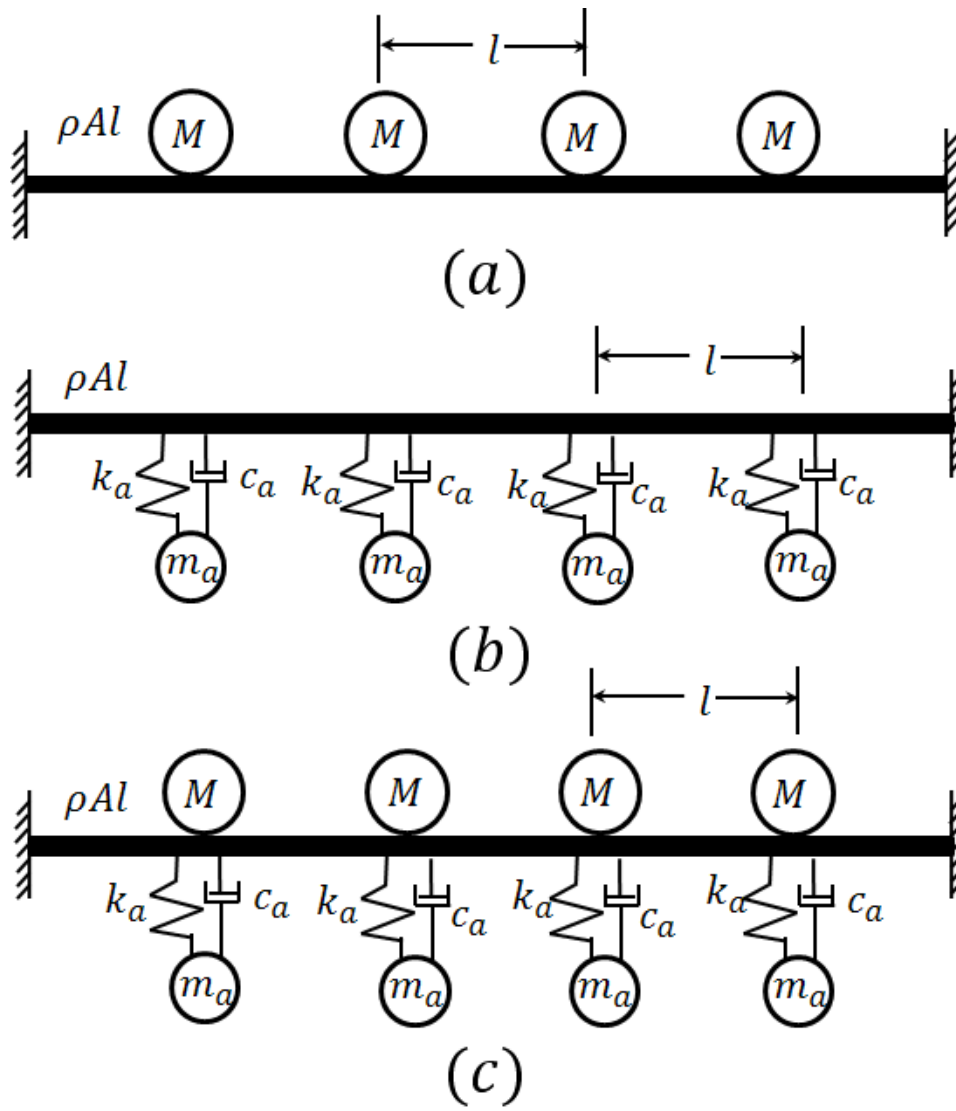
Figure 2.1: (a) Beam with periodically placed point masses. There are four masses with the masses at the ends assumed to be rigid (fixed). (b) Beam with periodic resonators. (c) Beam with two-fold periodicity.
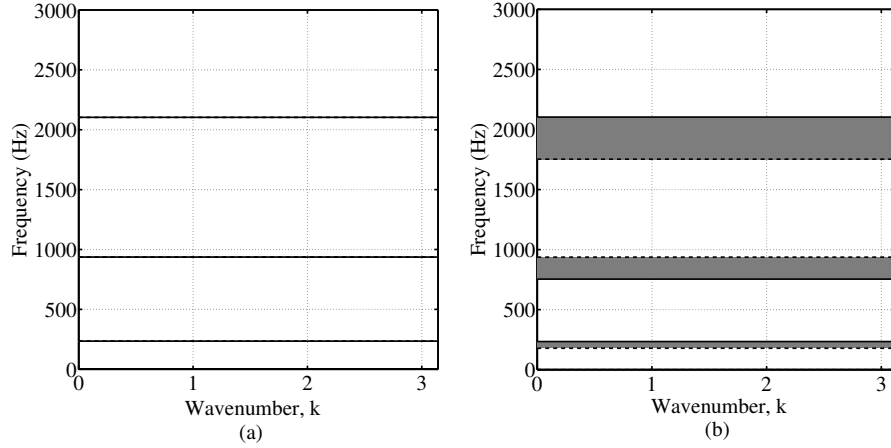
Figure 2.2: Bandgap formation in a beam. (a) Natural frequencies of a beam with no periodic inclusions plotted against the non-dimensional wavenumber, k.(b) Natural frequencies of a beam with periodic inclusions. The grey shades represent bandgaps. The dotted lines bounding the grey shades are the natural frequencies of the unitcell with guided boundary conditions and the solid lines bounding the grey shades are the natural frequencies of the unitcell with simply supported ends.

end and the odd modes of the simply supported end are further influenced by the addition of the resonator, with the even modes of the guided end rising along the frequency and the odd modes of the simply supported end falling with frequency, causing them to approach each other. This causes the narrowing of the bandgaps associated with the Bragg frequencies as shown in Figs 2.4(a) and 2.4(b).

2.3 Analysis of Wave Propagation using Bloch Theory

When a structure is periodic and infinite, Floquet-Bloch theorem or Bloch theorem takes advantage of the periodicity and the properties of the infinite structure can be investigated by considering the repeating unit. The result is the dispersion diagram displaying ranges of frequencies associated with pass and stop bands.

We shall now see how the Bloch theorem applies to a two-dimensional periodic system, which can be easily then applied to a one-dimansional system such as the
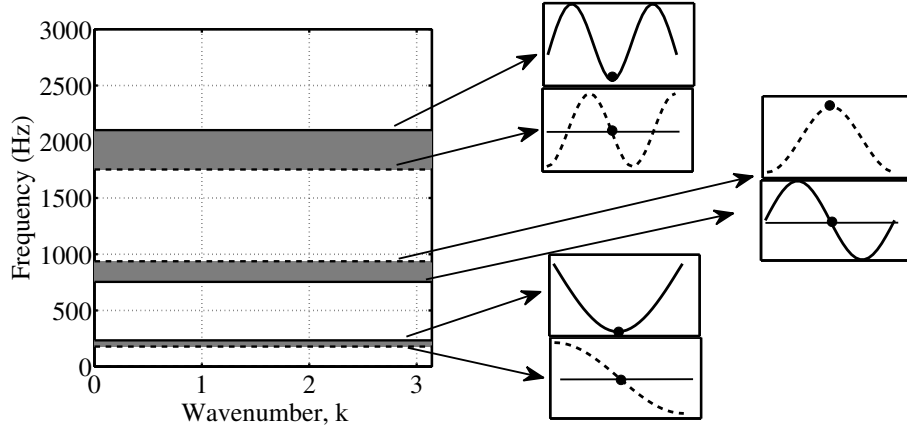
Figure 2.3: Schematic of bandgap formation. The mode shapes for the two types of end condition are shown. When a periodic inclusion is introduced, the position of the natural frequencies are not influenced if they coincide with the node position as indicated by the marker. The dotted lines correspond to the guided end natural frequencies and the solid lines correspond to the simply supported end natural frequencies.

ones we study in this work. Consider Fig 2.5(a). It depicts a unitcell of an infinite lattice. Tessellating this unitcell along the basis vectors $\mathbf{e}_i$, translates to a periodic structure with the unitcell as the repeating periodic unit. Let *A* be a point in the unitcell (see Fig 2.5(b)). Admitting a harmonic plane wave into the infinite system yields,

$$\mathbf{q}(\mathbf{r}) = \mathbf{q}_A e^{i(\omega t - \mathbf{k}.\mathbf{r})}. \tag{2.1}$$

where $\mathbf{q}$ is the displacement of the harmonic wave at a reference unitcell, $\mathbf{q}_A$ is the wave amplitude of the point A; ω is the frequency (rad/sec). This means that in order to determine the response at every unitcell, the problem size scales with the degree of freedom of the system. Bloch's theorem states that the displacement at any arbitrary point (say, B) in the unitcell with a position vector $\mathbf{r} = \mathbf{p} + n\mathbf{e}_i$ where, *n* represents the number of unitcell translations along vector direction $textbfe_i$ from *A* to a corresponding point *B* in a distant unitcell is given by,

21
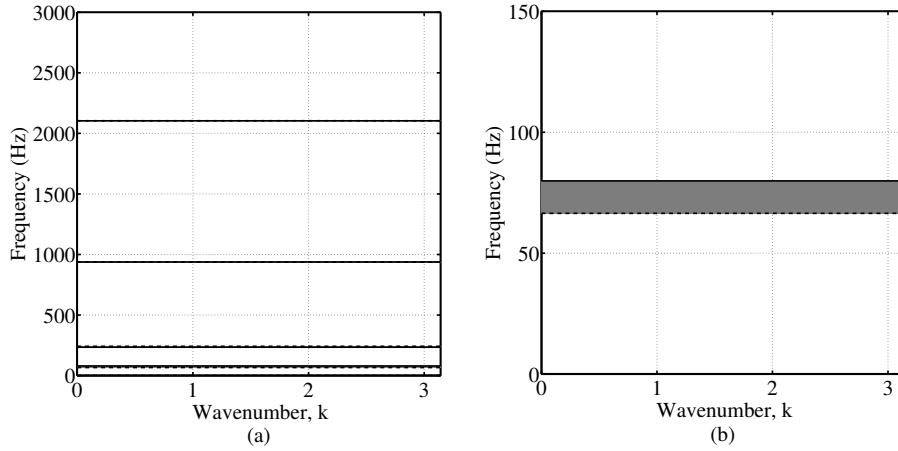
Figure 2.4: Bandgap formation in a beam with periodic resonators. (a) Natural frequencies corresponding to Bragg frequencies plotted against the non-dimensional wavenumber, k. (b) Natural frequencies corresponding to sub-Bragg frequencies. The grey shade represents a bandgap.

$$\mathbf{q}(\mathbf{r}) = \mathbf{q}_A(\mathbf{p})e^{-i(\mathbf{k}.(\mathbf{r}-\mathbf{p}))}. \tag{2.2}$$

where $\mathbf{q}_A(\mathbf{p})$ is the amplitude of A in the reference unitcell with a position vector ($\mathbf{p}$).

In simple terms, Bloch's theorem states that for any structure with repeating unitcells, the wave amplitude does not depend on the location of the unitcell within the periodic structure. Thus, one can understand wave propagation through the entire structure by considering the unitcell alone. Bloch's theorem thus leads to enormous savings in the analysis of wave propagation in periodic structures [6].

We illustrate the Bloch theorem on a periodic system sustaining a free harmonic wave propagation. The equations of motion of the unitcell are given by:

$$\mathbf{M}\ddot{\mathbf{q}} + \mathbf{K}\mathbf{q} = \mathbf{0}, \tag{2.3}$$

22

where, **M** and **K** are the assembled global mass and stiffness matrices of the unitcell respectively, obtained using Finite Element Method.
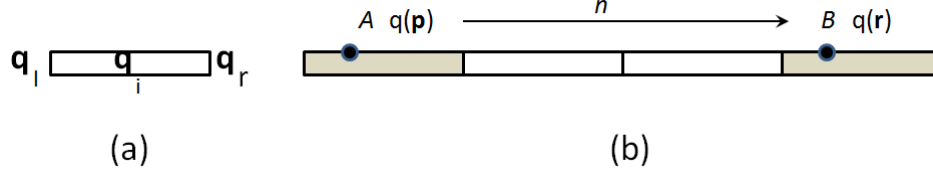
Figure 2.5: Explanation of Bloch theorem.(a) Unitcell of a periodic structure with displacements represented by **q** at the respective positions. The edges are the subscripts for **q**. (b) Represents a periodic structure formed by tessellating the unitcell through n translations. Point B is at the same position in its unitcell as the point A in the reference unitcell. The displacement q($\mathbf{r}$) of the point B can be represented in terms of the displacement of point A given by q($\mathbf{p}$).

We partition the unitcell edges as edge (l, r) and interior (I) degrees of freedom where l, r, correspond to the left and right degrees of freedom of the unitcell. Invoking Bloch's transformation [6] to the above equations of motion in Eq (2.2) we get,

$$\mathbf{q}_r = e^{-ik}\mathbf{q}_l; \tag{2.4}$$

We define a transformation:

$$\mathbf{q} = \mathbf{T}\tilde{\mathbf{q}}, \tag{2.5}$$

T as:

$$\mathbf{T}(k) = \begin{bmatrix} I & 0 & 0 \\ Ie^{-ik} & 0 & 0 \\ 0 & 0 & I \end{bmatrix} \text{ and}$$

using the above **T** matrix, one can represent Eq (2.4) as:

$$\mathbf{q} = \begin{bmatrix} \mathbf{q}_l \\ \mathbf{q}_r \\ \mathbf{q}_i \end{bmatrix} = \mathbf{T}(k) \begin{bmatrix} \mathbf{q}_l \\ \mathbf{q}_i \end{bmatrix} = \mathbf{T}(k)\tilde{\mathbf{q}}$$

Here, $\mathbf{T}$ is the Floquet-Bloch transformation matrix as a function of the wave vector component k along the direction of wave propagation. Now, applying Floquet-Bloch transformation to Eq (2.3) yields the eigenvalue problem in Bloch reduced co-ordinates $\tilde{\mathbf{q}}$ as:

$$\mathbf{T}^H\mathbf{K}\mathbf{T}\tilde{\mathbf{q}} - \omega^2\mathbf{T}^H\mathbf{M}\mathbf{T}\tilde{\mathbf{q}} = 0 \qquad (2.6)$$

where the superscript H denotes the Hermitian transpose. The solution to the eigenvalue problem defined above yields a relationship between the wave vector components k_1 and k_2 and frequencies ω. This can be depicted in the form of dispersion curves.

2.4 Effect of Local Resonators

As mentioned in Section 2.1, the bounding frequencies of the band edges of a periodic system correspond to the natural frequencies of the unitcell of the system with fixed and free boundary conditions. In this section, a string and a beam with attached local resonators will be analysed for the bounding frequencies of the band edges. Analytical expressions for the bounding frequencies will be derived using the *'Receptance Coupling'* technique and will be compared with the results obtained through dispersion curves. The effect of two-fold periodicity and the effect of damping on the bounding frequencies of the band edges will be presented subsequently.

2.4.1 Receptance Coupling Technique

Receptance is defined as the ratio of steady harmonic displacement response of a system to the harmonic input force [70]. Coupling a local resonator to a medium can be achieved by enforcing the necessary force equilibrium and displacement compatibility conditions expressed by receptance functions of individual subsys-

tems. Simple rules exist for coupling point receptances of two systems, each eval-
uated at the point of coupling. For two systems with point receptances H_1 and H_2,
the following rules can be stated:

$$\frac{1}{H} = \frac{1}{H_1} + \frac{1}{H_2}, \quad \text{parallel connection}$$
$$H = H_1 + H_2, \quad \text{series connection.}$$

(2.7)

The above rules provide the characteristic equations of the coupled system whose
solutions are the natural frequencies. We now apply the above rules to one-
dimensional systems such as a string and a beam with periodic resonators.

2.4.2 String with Periodic Resonators

As noted by Mead[17], to determine the bounding frequencies of a symmetric sys-
tem with periodically placed resonators, we need to determine the natural frequen-
cies of the unitcell of the system with pinned and guided boundary conditions.
Consider an infinite string with periodically placed resonators. The unitcell of this
system with the two types of end conditions is shown in Fig 2.6. The unitcell is
of length l. The oscillator is made up of a spring of stiffness k_a and mass m_a. The
tension in the string is assumed to be T.
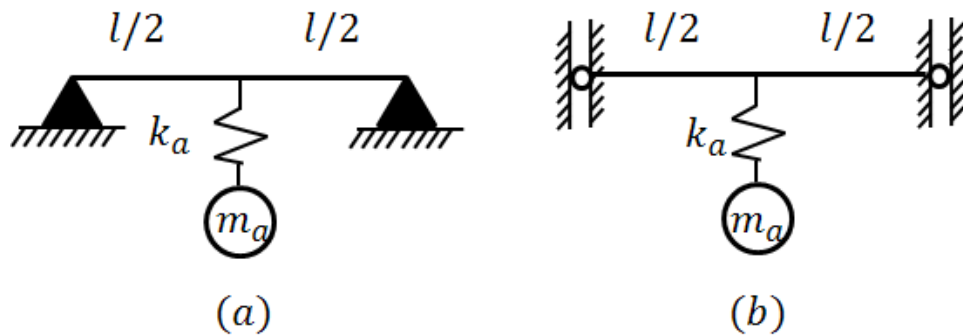
Figure 2.6: Unitcells of a string with attached spring-mass resonators. (a)
Unitcell of a string with pinned boundary conditions and (b) Unitcell of
a string with guided boundary conditions.

25

The width of the bandgap would therefore be the difference in the natural frequencies for the two types of end conditions. As given in [70], the receptance of a pinned-pinned string of length l with any unit attached in the middle is given as:

$$H_{string}\left(x = \frac{l}{2}\right) = \frac{\sin \lambda x \sin \lambda (l - x)}{T \lambda \sin \lambda l} = \frac{\sin^2 \lambda \frac{l}{2}}{T \lambda \sin \lambda l}, \tag{2.8}$$

where $\lambda = \omega \sqrt{\frac{m}{T}}$; ω is the natural frequency of the system and m is the mass of the string.

Receptance of a spring mass resonator can be written as:

$$H_{resonator} = -\frac{k_a - m_a \omega^2}{k_a m_a \omega^2} \tag{2.9}$$

Using

$$\frac{1}{H} = \frac{1}{H_{string}} + \frac{1}{H_{resonator}},$$

gives,

$$H = \frac{H_{string} H_{resonator}}{H_{string} + H_{resonator}} \tag{2.10}$$

Using Eq (2.8 and Eq (2.9) in Eq (2.10) gives us the characteristic equation:

$$k_a m_a \omega^2 \sin^2 \lambda \frac{l}{2} - T \lambda \sin \lambda l \left(k_a - m_a \omega^2\right) = 0. \tag{2.11}$$

We can simplify the above and solve to obtain approximate natural frequencies using $\sin \frac{\lambda l}{2} \approx \frac{\lambda l}{2}$ as:

$$\Omega_{ss} = \Omega_a \sqrt{\frac{1}{4 + \pi^2 \Omega_a^2 m_r}}, \tag{2.12}$$

where Ω is a non-dimensional frequency parameter and the suffix 'ss' corresponds to the simply supported condition; the non-dimensional frequency $\Omega_a = \sqrt{\frac{k_a l^2 m}{\pi^2 T m_a}}$, where the suffix '$a$' refers to the resonator and $m_r = \frac{m_a}{m}$ is the ratio of the mass of the resonator (m_a) to that of the unitcell of the string (m).

A similar analysis can now be performed on the unitcell with guided end boundary conditions with the receptance:

$$H_{string}\left(x = \frac{l}{2}\right) = -\left[\frac{\cos \lambda x \cos \lambda (l-x)}{T\lambda \sin \lambda l}\right]_{x=\frac{l}{2}} = -\frac{\cos^2 \lambda \frac{l}{2}}{T\lambda \sin \lambda l}, \quad (2.13)$$

where $\lambda = \omega\sqrt{\frac{m}{T}}$. Using Eq (2.13) and Eq (2.9) in Eq (2.10) we can obtain the characteristic equation for the natural frequencies as:

$$-k_a m_a \omega^2 \cos^2 \lambda \frac{l}{2} - T\lambda \sin \lambda l \left(k_a - m_a \omega^2\right) = 0. \quad (2.14)$$

The lowest resonance frequency is obtained through the approximation $\cot \frac{\lambda l}{2} \approx \frac{2}{\lambda l}$ and further simplifying the above equation yields,

$$\Omega_{guided} = \Omega_a \sqrt{1 + m_r}, \quad (2.15)$$

where the suffix '*guided*' corresponds to the guided end condition.

Finally, the width of the bandgap introduced by the local resonator will be

$$\Delta\Omega = \Omega_a \sqrt{1 + m_r} - \sqrt{\frac{1}{\frac{1}{\Omega_a^2} + \frac{m_r \pi^2}{4}}}$$

$$= \Omega_a \left[\sqrt{1 + m_r} - \sqrt{\frac{1}{4 + \pi^2 m_r \Omega_a^2}}\right] \quad (2.16)$$

Similar equations as above have been arrived at in [68] by solving the underlying partial differential equations. Finally, we note that for a fixed stiffness of the resonator (k_a), or given strength of coupling, increasing the mass contrast m_r will increase the local resonance bandgap, while lowering the bounding frequencies of the bandgap at the same time.

2.4.3 A Timoshenko Beam with Two-fold Periodicity

Fig 2.1(c) represents a finite beam with a two fold periodicity in the form of damped resonators in addition to masses on the beam. In this section we analyze the general case of two-fold periodicity with damping for predicting the bounding frequencies. The width of the bandgap is the difference in the natural frequencies of the unitcell for the two end conditions as shown in Fig 2.7. Point receptance of a beam at x can be expressed in terms of the normal mode shapes of the beam [70] as:

$$H_b = \sum_{r=1}^{n} \frac{\Phi_r(x)^2}{a_r(\omega_r^2 - \omega^2 + i2\zeta_r\omega\omega_r)},$$

(2.17)

where $\Phi_r(x)$ is the mode shape associated with the normal mode r with natural frequency ω_r and ζ_r is the damping ratio associated with mode r. The mass normalization constant is a_r. We choose to express in terms of the normal modes are we are interested in only the bounding frequencies and these are the natural frequencies of the unitcells with different constraints.

The receptance of the damped resonator is:

$$H_a = -\frac{k_a - m_a\omega^2 + ic_a\omega}{(k_a + ic_a\omega)m_a\omega^2},$$

(2.18)

where, k_a m_a and c_a correspond to the stiffness, mass and damping coefficient of the resonator respectively. Similarly, the receptance of the lumped mass M is given as:

$$H_m = -\frac{1}{M\omega^2}.$$

(2.19)

We can now use the systems in parallel coupling rule for the beam, resonator, and the mass since all of them have the same displacement at the point of coupling:

$$\frac{1}{H} = \frac{1}{H_b} + \frac{1}{H_a} + \frac{1}{H_m}$$

(2.20)

It must be pointed out that not all terms in the series expansion of the receptance in Eq (2.17) need to be considered. Now, in order to determine the natural
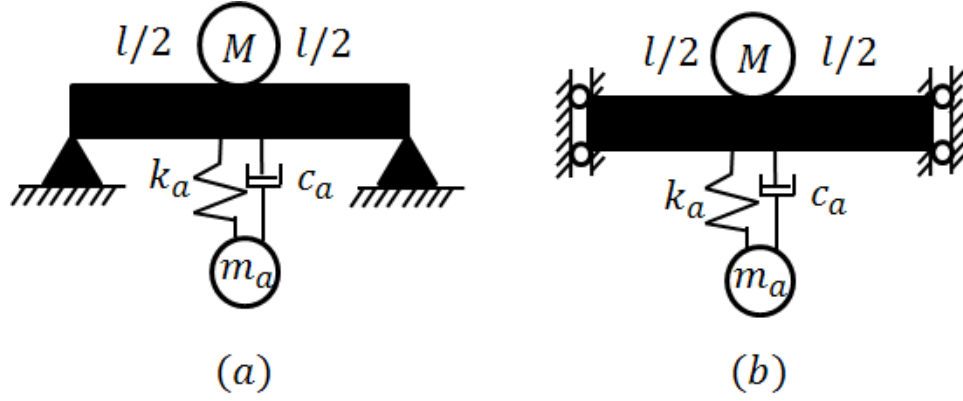
Figure 2.7: Unitcell of the beam with (a) Simply supported and (b) Guided
boundary conditions.

frequency of the simply supported unitcell as shown in Fig 2.7(a), we approximate
the receptance of the beam for $n = 1$ as:

$$H_b \approx \frac{\Phi_1(x)^2}{a_1(\omega_b^2 - \omega^2 + i2\zeta_b\omega\omega_b)}, \tag{2.21}$$

where $\Phi_1(x) = \sin\frac{\pi x}{l}$ is the first mode shape of the pinned-pinned beam and $\omega_b = \sqrt{\frac{\pi^4 EI}{\rho Al^4}}$, where E is the Young's modulus of the beam material, A is area of cross-section, I is second moment of area with respect to neutral axis. The normalization constant $a_1 = \frac{\rho Al}{2}$. Substituting Eqs (2.21), (2.18) and (2.19) in Eq (2.20) and after simplification, the characteristic equation governing the natural frequencies of the coupled system is obtained to be:

$$-2(k_a - m_a\omega^2 + ic_a\omega)M\omega^2 + (k_a - m_a\omega^2 +$$
$$ic_a\omega)\rho AL(\omega_b^2 - \omega^2 + i2\zeta_b\omega\omega_b) - 2m_a\omega^2(k_a + ic_a\omega) = 0.$$

If we ignore the damping in the beam $\zeta_b = 0$, the equation above can be solved
for the natural frequency as:

$$\omega_{ss} = \omega_a \frac{(2p+1+r^2+2m_r) \pm \sqrt{(2p+1+r^2+2m_r)^2 - 4(2p+1)r^2}}{(4p+2)} \quad (2.22)$$

where ω_{ss} stands for the natural frequency of the beam with simply supported end condition, p is the ratio of the mass M to the mass of the beam m_b, r is the ratio of the frequency of the beam to that of the resonator and m_r is the ratio of the mass of the resonator to that of the beam. Choosing the appropriate root gives us the natural frequency of the simply supported beam and thereby the lower bound of the bandgap. It can clearly be seen from the above equation that for a given beam, the natural frequency of the system is a function of ω_a. Therefore by varying the mass and stiffness of the resonator it is possible to achieve a desired bounding frequency of the bandgap.

Performing a similar analysis using the receptance of the guided beam, shown in Fig 2.7(b), will give the second bound for the bandgap. Note that we can't ignore the rigid body mode of the beam since the resonator gives finite potential energy for any motion. The one term series approximation of the receptance function for the guided beam around zero frequency is:

$$H_b = \frac{1}{\rho A L(-\omega^2)}, \quad (2.23)$$

By following the same procedure as used in simply-supported case, the characteristic equation is:

$$(k_a - m_a \omega^2 + ic_a \omega) M \omega^2 + (k_a - m_a \omega^2 +$$
$$ic_a \omega) \rho A L \omega^2 + m_a \omega^2 (k_a + ic_a \omega) = 0 \quad (2.24)$$

For an undamped case, the non-zero natural frequency is:

$$\omega_{guided} = \omega_a \sqrt{1 + \frac{m_r}{(1+p)}} \quad (2.25)$$

Thus the natural frequency of the unitcell of the system is once again dependent on the frequency of the resonator. The width of a bandgap is the difference between the natural frequencies of the guided and simply supported unitcells given by:

$$\triangle \omega = \omega_a(\sqrt{1 + \frac{m_r}{(1+p)}} -$$
$$\frac{(2p+1+r^2+2m_r) \pm \sqrt{(2p+1+r^2+2m_r)-4(2p+1)r^2}}{(4p+2)}). \qquad (2.26)$$

Varying the mass and stiffness of the resonator will facilitate to increase the width of the bandgap.

2.5   Analysis of Bandgaps in Periodic Timoshenko Beams

In this section we shall determine the band structure for the unitcells of the systems shown in Fig 2.1. In each of the dispersion curves to be plotted, the horizontal solid lines bounding the grey shades correspond to the natural frequency of the unitcell with simply supported ends and the dotted lines shall correspond to the natural frequencies of the unitcell of the system with guided end boundary conditions. Transmission Frequency Response Functions (FRF's) for the finite systems will also be shown. While transitioning from an infinite system to a finite system, it is important to note that the unitcell analysis is for an infinite system. The points on the dispersion curves will therefore be continuous. A finite system will have a finite number of resonant frequencies corresponding to the number of unitcells in the finite system. These resonant frequencies would be distinct points along the dispersion curves [72] as shown in Fig 2.8. Increasing the number of unitcells would increase the number of points along the dispersion curves, making it more continuous. However, the position of the band gaps would be unaffected by the addition of the unitcells as can be seen from Fig 2.9.

Employing the Bloch formulation elucidated in Section 2.3, the dispersion curves for the unitcell of the system shown in 2.1(a) is shown in Fig 2.10. It may be observed that for this system, the Bragg frequencies exhibit characteristic pass and stop bands (Fig 2.10(a)), while the sub-Bragg frequencies do not show any
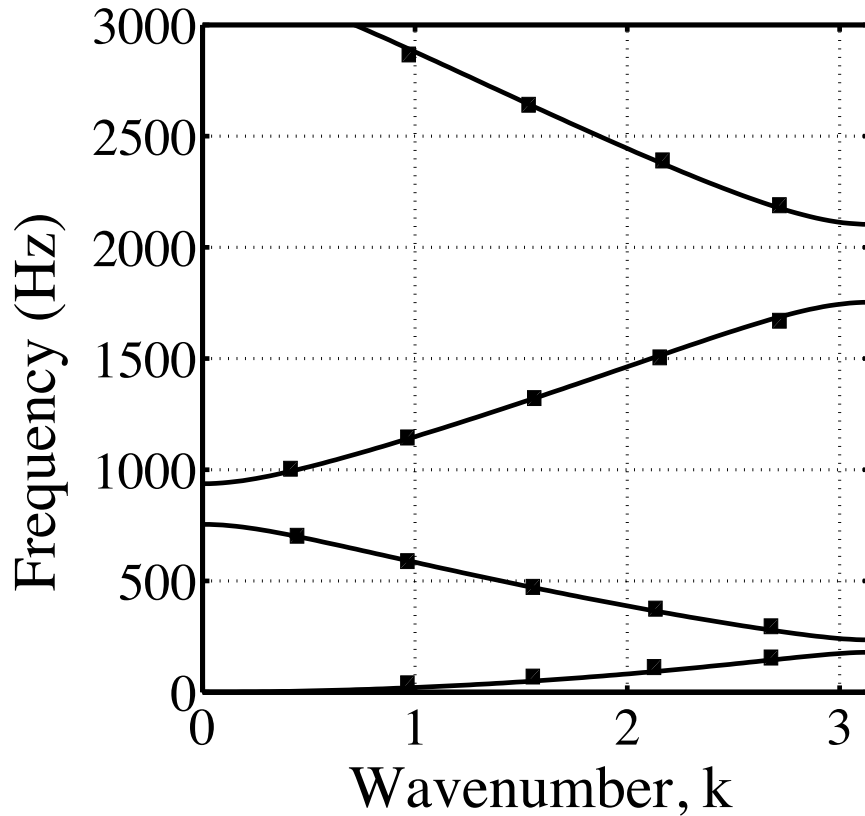
Figure 2.8: Dispersion curves for an infinite system showing descrete points of the finite system. The number of points along the dispersion curves increases with increasing number of unitcells. However, the position of the bandgaps are unaffected.

bandgaps (Fig 2.10(b)). We choose a target frequency of 70 Hz which lies in the first pass band of the system (indicated by the solid line). Our aim is to create a bandgap at this target frequency.

On introducing resonators, each with a resonant frequency of 70 Hz, we can create a bandgap at the target frequency. We therefore plot the dispersion curves corresponding to the unitcell of the system shown in 2.1(b). The dispersion curves for this system are shown in Fig 2.11. We observe that the bandgaps corresponding
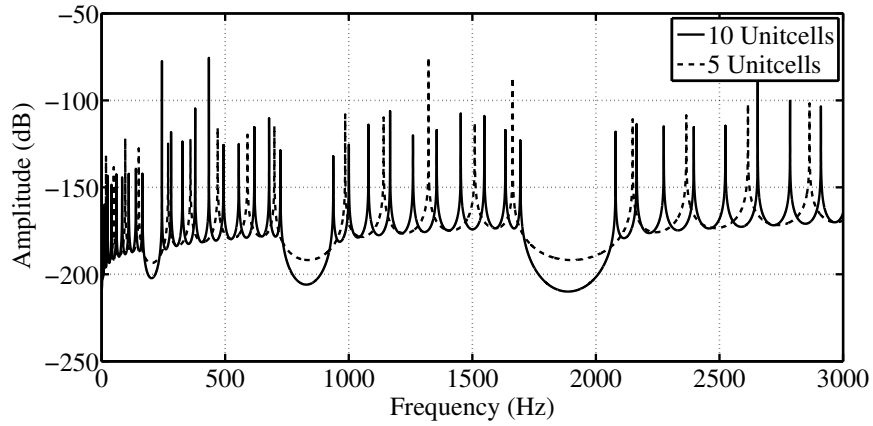
Figure 2.9: Frequency response functions for a beam with 5 unitcells and 10 unitcells. The position of the bandgaps are unaffected by increasing the number of unitcells. The number of resonant frequencies in each passband correspond to the number of unitcells in the system.
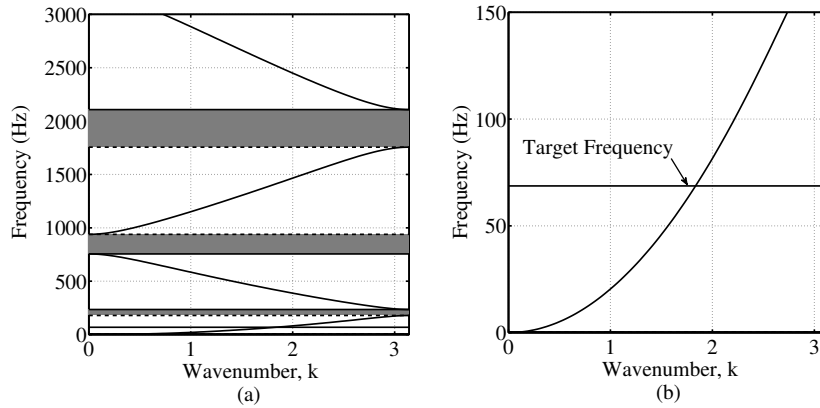
Figure 2.10: Dispersion curve for a beam with periodic masses. (a) Bragg frequencies; (b) Sub-Bragg frequencies. The system shows pass and stop bands at Bragg frequencies. We intend to create a bandgap at the sub-Bragg frequency, at a frequency indicated by the Target Frequency (70 Hz)

33

to Bragg frequencies have narrowed down, while a sub-Bragg bandgap at the target frequency has been created.
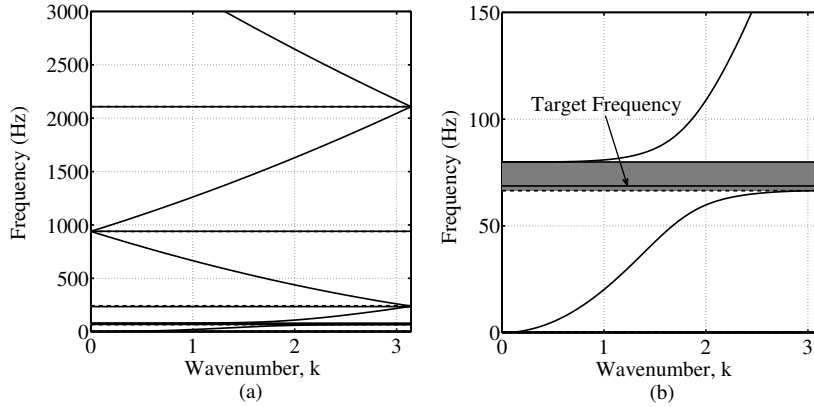
Figure 2.11: Dispersion curve for a beam with periodic resonators. (a) Bragg frequencies; (b) Sub-Bragg frequencies. The system shows no pass and stop bands at Bragg frequencies. A bandgap at sub-Bragg frequencies, corresponding to the resonant frequency of the resonator is created.

On introducing two-fold periodicity as shown in Fig2.1(c), we find that the bandgaps corresponding to the Bragg frequencies open up, while preserving the local resonant bandgap.

The transmission FRF's for each of the systems shown in Fig 2.1 are shown in Figs 2.13, 2.14 and 2.15, respectively. The force input is near the left end of the system while the displacement response is measured near the right end. Band structures similar to those exhibited by the infinite system (dispersion curves) are seen. As can be seen from Fig 2.14b, there is a shift in the anti-resonance away from the target frequency. Interferences between the scattering of the resonant modes and the propagating waves causes the shift of the anti-resonance as well as the asymmetry. This is commonly called Fano interference, as noted in [29, 73]. Correspondingly, a bandgap of 15 Hz at the target frequency is formed.

The effect of varying the mass of the resonator while maintaining the mass of the beam constant can be seen from Fig 2.16. In order to preserve the same tar-
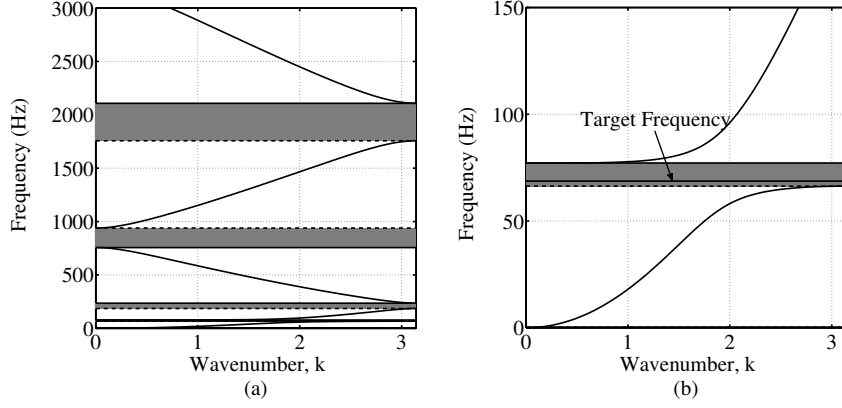
Figure 2.12: Dispersion curve for a beam with periodic masses and resonators. (a) Bragg frequencies; (b) Sub-Bragg frequencies. The system shows pass and stop bands at Bragg frequencies while preserving the local resonant bandgap.

get frequency, the stiffness of the spring has to be proportionally increased such that $\sqrt{\dfrac{k_a}{m_a}}$ remains the same. This results in an increase in the guided end natural frequency, while the simply supported end natural frequency decreases. This consequently results in an increase of the bandgap. Thus, in order to achieve the widest possible bandgap, ideally the stiffness and mass of the attached resonators should be as high as possible. A surface plot showing the influence of mass ratio, stiffness ratio (ratio of the resonator stiffness to the beam stiffness) and the width of the bandgap is shown in Fig 2.17.

2.6   Effect of Damping on Local Resonance Bandgaps

In this section, the effect of damping on the bandgaps is determined. The damped dispersion curves are obtained by two methods - State space method and Rayleigh perturbation. Finally, the effect of changing the parameters of the resonator on the damped dispersion curves will be presented.
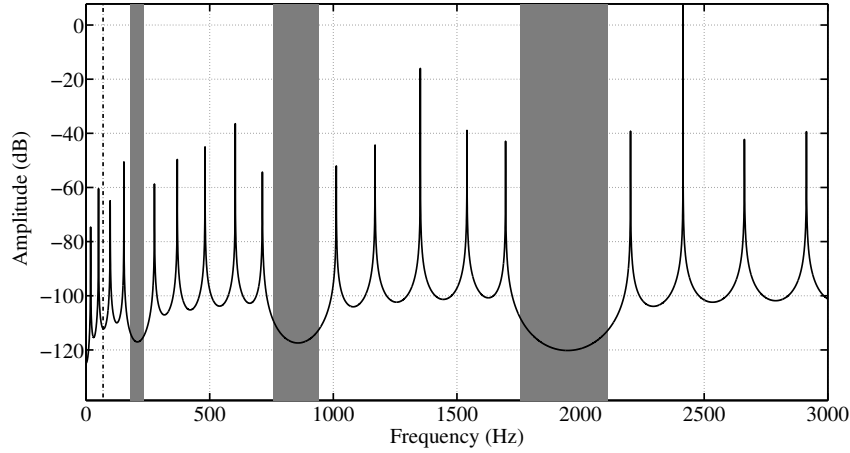
(a) FRF corresponding to Bragg frequencies
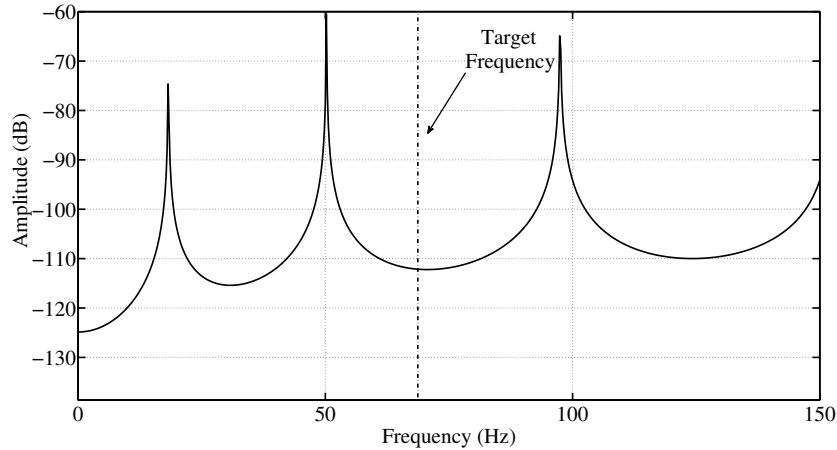
(b) FRF corresponding to sub-Bragg frequencies

Figure 2.13: Transmission FRF of a beam with periodically placed point masses. Input to the beam is at a point 5 cm from one end, while the response is evaluated at 5 cm from the opposite end. Pass and stop bands are clearly revealed at Bragg frequencies with each pass band showing five modes, corresponding to the degree of freedom of the system. No sub-Bragg bandgaps are seen.

We assume a linear damping model such that the damping matrix is proportional to the mass and stiffness matrices i.e. $\mathbf{C} = \alpha \mathbf{M} + \beta \mathbf{K}$.
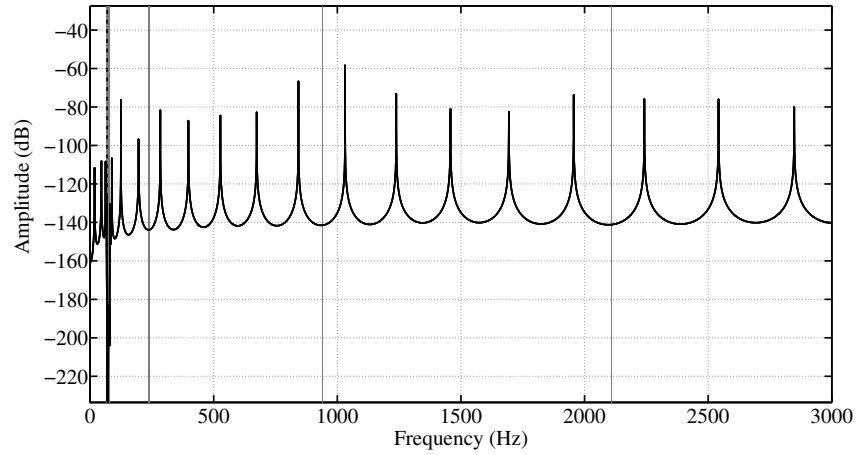
36

(a) FRF corresponding to Bragg frequencies
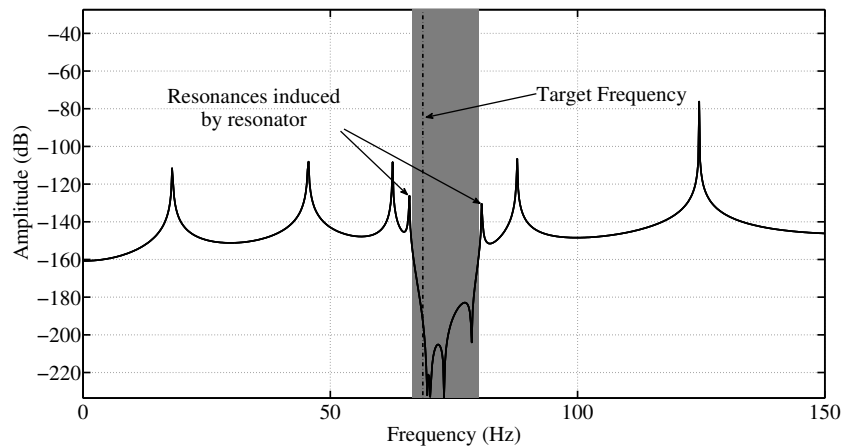
(b) FRF corresponding to sub-Bragg frequencies

Figure 2.14: Frequency response function of a beam with periodically placed spring mass systems. An anti resonance is formed close to the target frequency. The asymmetry in the bandgap and the shift in the anti-resonance is attributed to Fano interferences. It may also be observed that the bandgaps corresponding to the Bragg frequencies do not exist any more. Additionally, two new resonant frequencies are formed due to the resonator.
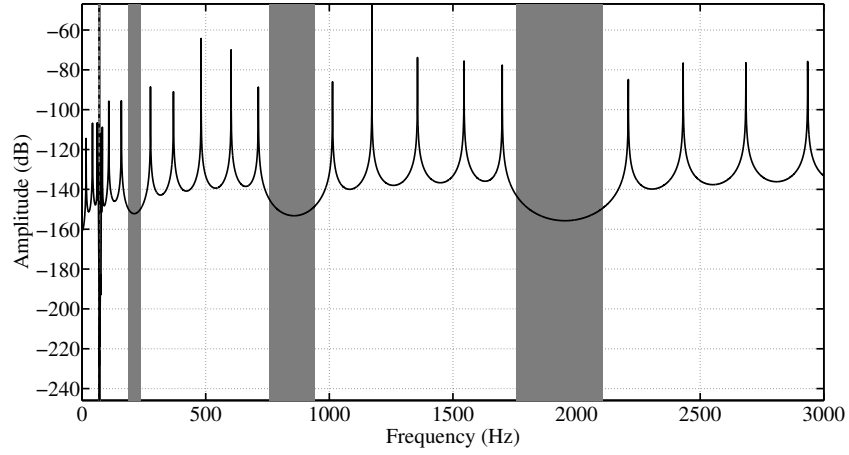
(a) FRF corresponding to Bragg frequencies
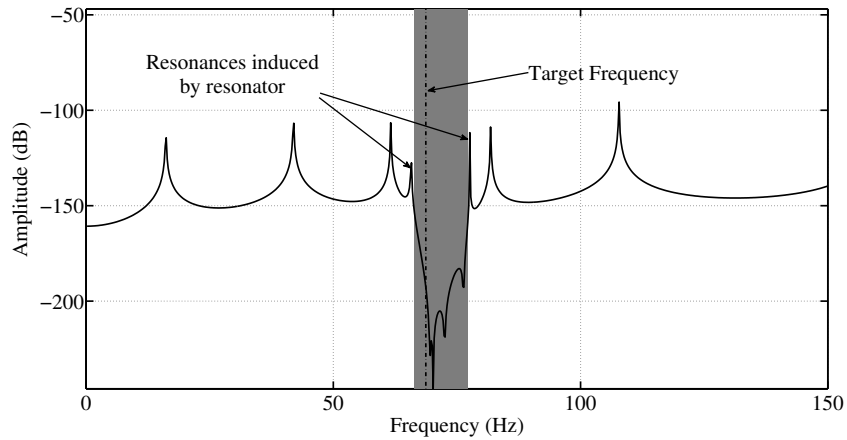
(b) FRF corresponding to sub-Bragg frequencies

Figure 2.15: Transmission FRF of a beam with two-fold periodicity. The dotted vertical line corresponds to the target frequency (70 Hz). A local resonant bandgap is formed around the resonant frequency. At the same time, the bandgaps corresponding to the Bragg frequencies are recovered.

Bloch reduced matrices are usually solved for the eigenvalues and eigenvectors to yield the band structure. However with damping, the equations are of the form [74]:
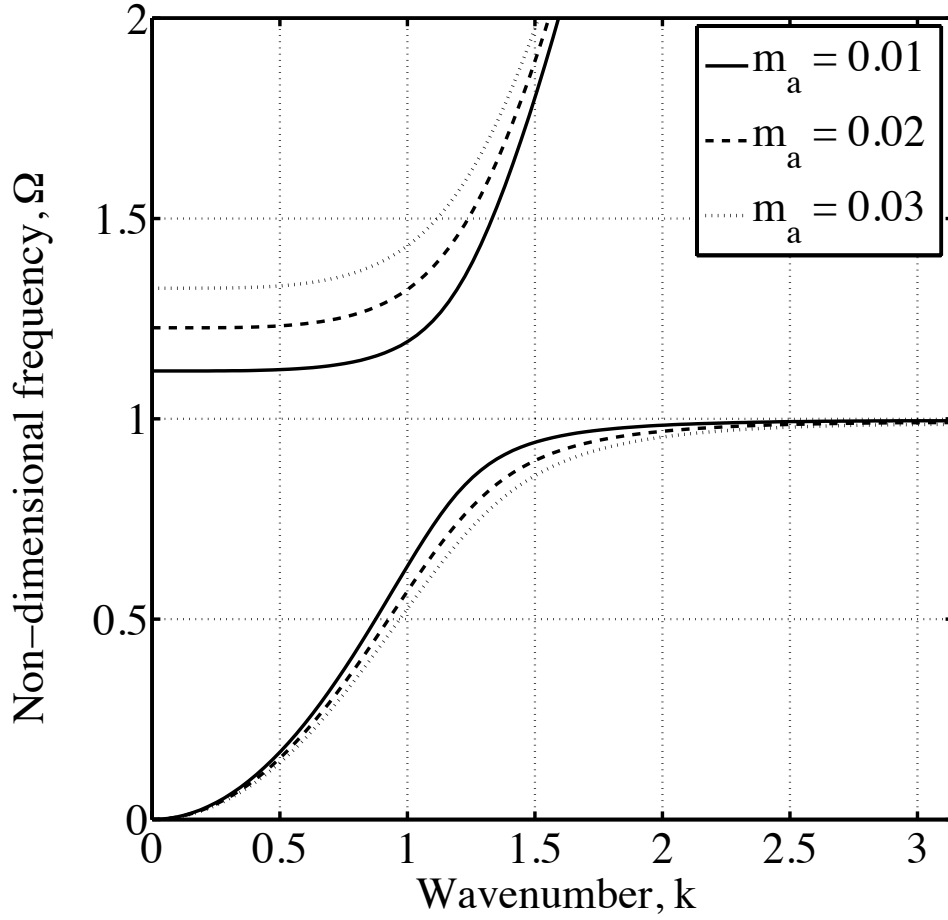
Figure 2.16: Dispersion curve for varying mass of the resonator. The width of the bandgap increases for increasing mass of the resonator. m_a corresponds to the mass of the resonator, m_b corresponds to the mass of the beam and is constant at 0.0394 kg and Ω is the non-dimensional frequency parameter.

$$\mathbf{M}\ddot{\mathbf{x}}(t) + \mathbf{C}\dot{\mathbf{x}}(t) + \mathbf{K}\mathbf{x}(t) = 0, \tag{2.27}$$
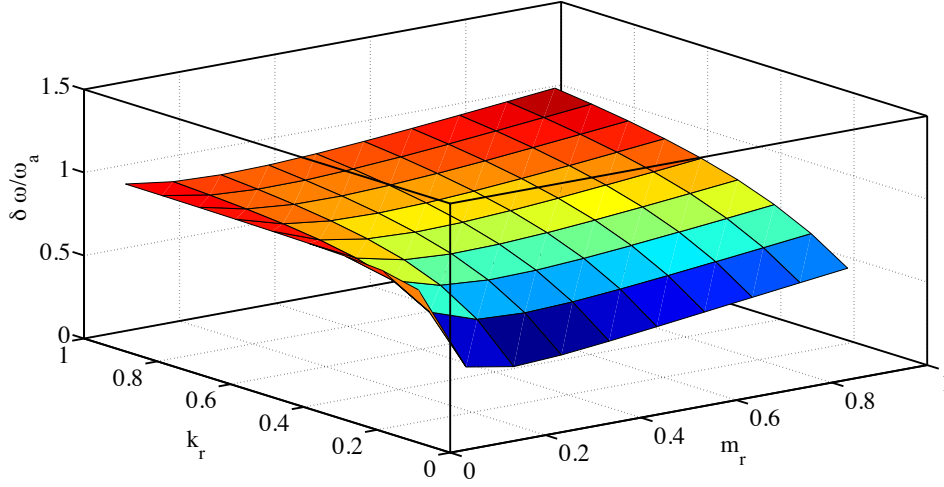
Figure 2.17: Surface plot depicting the influence of stiffness and mass ratios on the width of the bandgap. The greatest width of the bandgap is attained when both stiffness ratio and mass ratio are the highest.

Eq (2.27) cannot be solved directly for the eigenvalue problem because of the extra term introduced by the damping. Damped Bloch waves has been studied previously [74]. Two approaches for solving damped Bloch waves have been presented by [74], [75]: the state space method and the Rayleigh perturbation method. We shall first look into the state space approach.

2.6.1 State-Space Analysis

In the state space method, we convert Eq (2.27) into a linear, asymmetric eigenvalue problem by introducing a state vector. Let

$$\mathbf{q} = \left[\begin{array}{c} \mathbf{q}_1(t) \\ \mathbf{q}_2(t) \end{array} \right] = \left[\begin{array}{c} \mathbf{x}(t) \\ \dot{\mathbf{x}}(t) \end{array} \right].$$

Introducing the above in the equations of motion of the unit cell Eq 2.27

$$\Rightarrow \dot{\mathbf{q}}_2 = -\mathbf{M}^{-1}\mathbf{C}\dot{\mathbf{x}} - \mathbf{M}^{-1}\mathbf{K}\mathbf{x}$$

$$\Rightarrow \dot{\mathbf{q}}_2 = -\mathbf{M}^{-1}\mathbf{C}\dot{\mathbf{q}}_2 - \mathbf{M}^{-1}\mathbf{K}\mathbf{q}_1. \tag{2.28}$$

40

Eq (2.27) can be written in the state form as:

$$\dot{\mathbf{q}} = \mathbf{A}\mathbf{q},$$

where,

$$\mathbf{A} = \begin{bmatrix} \mathbf{0} & \mathbf{I} \\ -\mathbf{M}^{-1}\mathbf{K} & -\mathbf{M}^{-1}\mathbf{C} \end{bmatrix}$$

The eigenvalue problem can now be set up as:

$$\mathbf{A}\mathbf{q} = \lambda\mathbf{q}. \tag{2.29}$$

The eigenvalues obtained from the Eq (2.29) are either real or complex conjugates. Using the above analysis and combining with the Bloch transformation for the unitcell, it is possible to obtain damped Bloch waves. Using the **A** matrix defined in Eq (2.6.1) to set up a state space eigenvalue problem, the system is solved and the real and imaginary parts of the damped bloch waves can be plotted.

2.6.2 Rayleigh Perturbation Method

This method has a distinct advantage over the state space approach in that the size of the matrix to be solved for the eigenvalues remains the same as that of the undamped system. In this method, the undamped mass and stiffness matrices are Bloch reduced and the undamped frequencies of the system are first extracted. For proportional damping case, i.e., when $\mathbf{C} = \alpha\mathbf{M} + \beta\mathbf{K}$, the damped frequencies (as given in [75]) can simply be written as

$$\lambda_n = -\zeta_n\omega_n + i\omega_n\sqrt{1 - \zeta_n^2}, \tag{2.30}$$

where,

$$\omega_n = \sqrt{\frac{\mathbf{u}_n^T\mathbf{K}\mathbf{u}_n}{\mathbf{u}_n^T\mathbf{M}\mathbf{u}_n}}; \zeta_n = \frac{\mathbf{u}_n^T\mathbf{C}\mathbf{u}_n}{2\omega_n}. \tag{2.31}$$

ω_n stands for the undamped natural frequencies of the system. The resulting damped frequencies are complex and the real and imaginary parts of the system can be plotted.

41

2.6.3 Results

Either of the methods may be used for plotting the dispersion curves. It is important to note that the beam is always under damped in our analysis. The variation in the width of the bandgap as a function of the resonator's damping coefficient, for a fixed value of damping for the beam is shown in Fig 2.18. It can be seen that for a particular value of ζ of the resonator, the bandgap ceases to exist. Thus, there exists an optimum value of ζ beyond which one cannot obtain a width for the bandgap. A trade-off should be made between the mass of the resonator that can be used and the damping value of the resonator to obtain the best possible width of the resonant bandgap.

2.7 Summary

Linear analysis of systems with periodicity has been conducted. The systems considered were second order systems such as strings and fourth order Timoshenko beams with periodicity. Finite element method was employed to study the systems. Wave propagation analysis using Floquet-Bloch theorem was conducted for these systems which revealed the existence of pass and stop bands which occur alternately. Regardless of the type of periodicity or the order of the system, similar band structure will be obtained. Local resonators such as spring-mass systems help in creating bandgaps at a desired frequency (corresponding to the resonance frequency of the attached resonators) which lie below the Bragg frequencies. However, this results in a closure of bandgaps corresponding to the Bragg frequencies. On the other hand, if a two-fold periodicity is maintained in the system, one achieves a bandgap around the desired frequency while preserving the bandgaps corresponding to the Bragg frequencies.

The bounding frequencies of bandgaps of periodic structures correspond to the natural frequencies of the unitcells of the system with their ends fixed or free. Analytical expressions which were derived using the receptance technique verified the same. The analysis showed that the bounding frequencies depend on the parameter values of the attached resonators. Thus, by changing the parameters of the attached resonators, it is possible to tailor the width of the bandgap. It was seen that increasing the mass of the attached resonator increases the width of the bandgap. In order
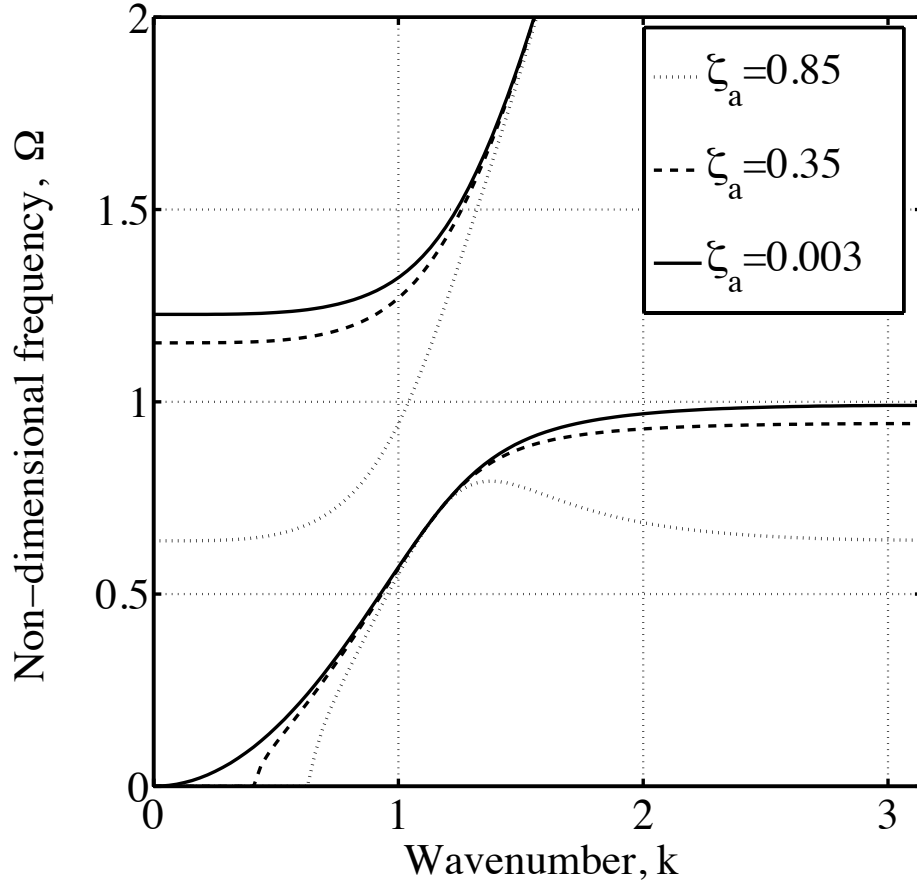
Figure 2.18: Dispersion curves for varying values of the resonator damping (ζ_a) for a given underdamped beam ($\zeta_b = 0.4$). The curves fall in value for increasing values of damping until a certain value beyond which the resonant bandgap ceases to exist.

to maintain the same target frequency for bandgap creation, the stiffness of the resonator has to be increased proportionately. This implies that for the widest possible gap, ideally the resonator should be as stiff and as heavy as possible.

The effect of damping on local resonance structures was further explored. The receptance technique yielded solutions for the bounding frequencies of the bandgaps. Dispersion curves for damped systems was obtained using two techniques - The state space method and the Rayleigh perturbation method. The effect

of varying damping on the system was explored. The effect of increasing the damping of the resonator for a given under damped beam was to decrease the width of the bandgap. There exists a cut-off value of the damping of the resonator beyond which one loses the bandgap at the desired resonance frequency. Thus, one has to carefully choose the right mass, stiffness and damping values for the attached resonator in order to achieve the desired width of the bandgap.

This chapter considered the wave propagation in the linear domain. Result were obtained using finite element techniques. In the forthcoming chapter, experiments will be presented to verify the above theoretical results.

Chapter 3

Experiments

3.1 Introduction

In Chapter 2 we analysed propagation of linear waves in a beam with periodically placed masses. It was seen that the effect of periodicity on the beam was to introduce regions of pass bands and stop bands corresponding to the zones of propagation and attenuation of travelling waves, respectively. It was noted that each pass band contains as many resonant peaks as the number of bays or units, which corresponded to the degree of freedom of the system. Additionally, the effect of attaching local resonators to a beam and the effects of two-fold periodicity on the beam were investigated. The aim of the present chapter is to validate our theoretical predictions experimentally. To this end, we test the wave propagation characteristics on a beam with periodically placed idealized point masses by measuring the natural modes of vibrations of a finite system. Recall that natural modes fall within the passaband as shown in Fig 2.8. We then replace these point masses with spring-mass resonators and determine the characteristics of this system. Thereafter, we introduce a symmetric two-fold periodicity on the beam and subsequently, the effect of an asymmetric two-fold periodicity will be studied.

The chapter begins with a validation of the Finite Element (FE) results obtained from MATLAB© by verification through the data obtained from an FE package, ABAQUS© in Section 3.2. Introduction to the experimental set-up and a descrip-

tion of the experimental procedure is provided in Section 3.3. This is followed by a discussion of the results in Section 3.4. Conclusions are given in Section 3.5.

3.2   Finite Element Modelling

The main aim of this exercise is to validate our MATLAB© generated codes. Frequency Response Functions (FRFs) can be presented using FE models or may be obtained through experiments. A beam with point masses was analysed using finite element analysis in MATLAB© in Chapter 2. We verify our model by testing a beam of length 0.9 metres, with 8 pointmasses each weighing 20 gm placed periodically along it. Validation through an FE package, ABAQUS© is performed. The model is shown in Figs 3.1 and 3.2.
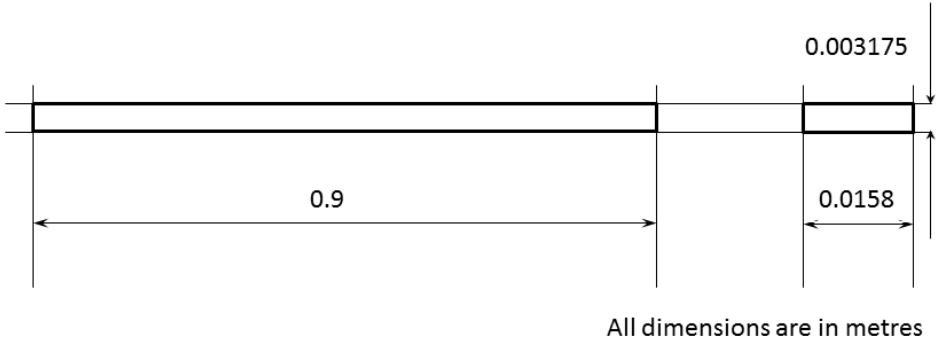

Figure 3.1: Dimensions of the beam.
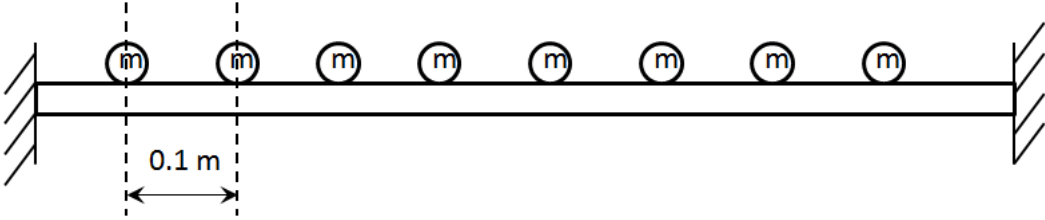
Figure 3.2: Beam with point masses.

The FE model of the setup was first simulated in MATLAB©. The beam was considered to be a Timoshenko beam and the natural frequencies of the beam were

computed using FE methods. Transfer FRF for a unit impulse given to the beam were noted. Here the impulse was given near the left end and the response was measured near the right end. The results obtained were verified by making use of a robust FE package such as ABAQUS©. The FE method used in MATLAB© needs to be checked for convergence. The mesh size used in MATLAB© for simulations is much lesser than the capacity of a robust software. Since MATLAB© was used in arriving at the solutions, it was necessary to validate the soundness of our model.

A 2-D beam model is first set up in ABAQUS© FE. Same dimensions as those used in MATLAB© are used here. The dimensions and material properties used are shown in Table 3.1. Fixed boundary conditions are assumed. Point masses each of 20 gm are placed periodically along the beam. The beam is meshed with homogeneous tetrahedral elements. Frequency analysis can be performed using Lanczos Eigensolver in ABAQUS© in the linear perturbation procedure. The natural frequencies are now compared with the results obtained from MATLAB. The comparison is shown in Table 3.2. There is excellent agreement for the first 20 modes, which gives us confidence on our analytical model.

Dimensions/Properties	Values
Element Type	2-D triangular Beam element
Length	0.9 m
Width	0.0158 m
Thickness	0.003175 m
Point mass	0.02 kg
Material	Steel
Density	7850 kg/m^3
Young's Modulus	210 GPa
Poisson's Ration	0.3

Table 3.1: Dimensions and material properties for the beam

As can be observed from Table 3.2, a huge gap lies between frequency numbers 8 and 9 which suggests the possibility of a bandgap here. After 9 frequencies (also the number of unitcells in this model), a similar gap is seen between the frequency numbers 17 and 18, suggesting the possibility of an existence of a bandgap here. Thus a bandgap hereafter occurs after every 9 frequencies which corresponds to the number of bays in the system.

47

S.No:	MATLAB©	ABAQUS©
1	17	16.9
2	46.8	46.8
3	91.6	91.6
4	151.3	151.3
5	225.1	225.1
6	311.7	311.7
7	405.7	405.7
8	489.1	489.0
9	798.1	798
10	925.9	925.7
11	1087.8	1087.4
12	1270.1	1270.0
13	1467.3	1466.6
14	1675.0	1674.0
15	1885.6	1884.3
16	2081.6	2080.1
17	2224.5	2223.7
18	2873.5	2871.7
19	3051.8	3049.3
20	3268.0	3266.0

Table 3.2: Natural frequencies for the periodic beam shown in Fig 3.2. MAT-LAB© and ABAQUS© models display similar natural frequencies.

To obtain FRFs from ABAQUS©, the data from ABAQUS© is obtained as a '.txt' file which is further post processed to obtain the relevant FRFs. Figure 3.3 shows a comparison between the FRFs obtained from MATLAB© and ABAQUS© models. As can be seen, the FRFs match very well for both models which gives us further confidence in our model. It may also be noted that each of the passbands exhibit 9 peaks, corresponding to the 9 resonant modes, which arise due to the 9 bays in the model. Bandgaps are observed after passband. Here there is exponential attenuation of the propagating waves.
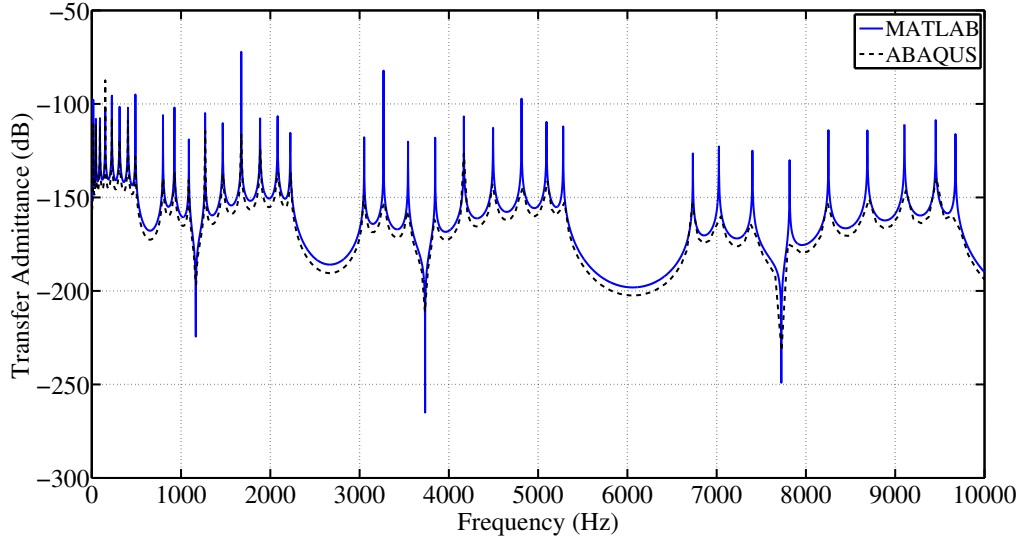
Figure 3.3: Frequency Response Function comparison graph between the MATLAB© and ABAQUS© models for a regular arrangement of the masses on the beam. Here, the impulse force is given at the location of the first point mass near the left end and the response is taken at the the third node from the right end.

3.3 Experiments

Now that our FE modelling in MATLAB© has been validated, we proceed to perform experiments on a one-dimensional beam. We consider four different cases to validate our findings. We shall investigate the effect of a beam with attached masses, attached resonators and the effects of two-fold periodicity as shown in Fig 3.4.

3.3.1 Experimental Setup

We consider a low carbon steel beam (density 7530 kg/m^3, Young's modulus 206.8 GPa) of length 0.9 m, width 19.1 cm and thickness 3.2 cm which is fixed at its two ends. Point masses are idealised in the form of steel spheres weighing 28.5 gm each. Four masses are placed at a distance of 0.18 m from each other. Local resonators are realized by means of a spring mass system, with the spring being a

49

closed-end and grounded compression type made of steel music wire of stiffness constant 5534 N/m (Model:9657K317L, Catalogue 1220) and weighing 3 gm.

The first set-up is that of a beam with periodically placed masses. For this purpose, the finite beam is placed with masses each of 28.5 gm placed at a distance of 0.18 m from each other as shown in Fig 3.4a.

The second set-up is that of the beam with periodically placed resonators. The masses which are each 28.5 gm are attached to the compression springs and these spring mass systems are attached to the beam at a distance of 0.18 m from each other as shown in Fig 3.4b.

The third set-up is that of a beam with a symmetric two-fold periodicity. Here, symmetric refers to the same mass on the resonator and on the beam. To achieve this, 4 additional masses each of 28.5 gm are attached exactly below the spring masses as shown in Fig 3.4c.

Lastly, an asymmetric two-fold periodicity is achieved by replacing the masses on the beam (28.5 gm) with masses each of 56.5 gm attached exactly below the spring mass systems as shown in Fig 3.4d.

Modal tests using an instrumented impulse hammer are performed on the set-up. An accelerometer is used to detect the response of the resulting vibrations. The analysis would provide information on the transmission FRFs.

3.3.2 Experimental Procedure

The schematic explaining the experimental procedure is shown in Fig 3.5. An impulse is delivered to the beam mass setup by means of the impulse hammer at its one end. An accelerometer placed at the other end of the beam senses the vibrations and the sensor signal is delivered to the signal conditioner. The conditioned signal is now passed through an inbuilt data acquisition system. An in-house data logging and post processing written in MATLAB© is used to analyse the acquired data.

An impulse hammer is a hammer with a force transducer at its end. The impulse hammer excites the test structure with equal force over a range of frequencies. An ideal impulse is of infinitesimally small duration of contact. In practice however, the contact time is small and finite. The duration of the contact time influences the frequency content of the force, with a larger contact time causing a

50

(a) Beam with periodic masses
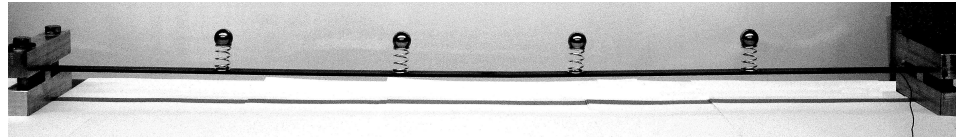
(b) Beam with attached resonators
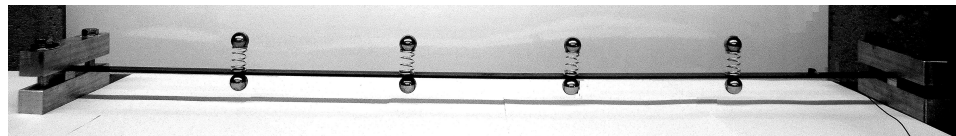
(c) Symmetric two-fold periodicity
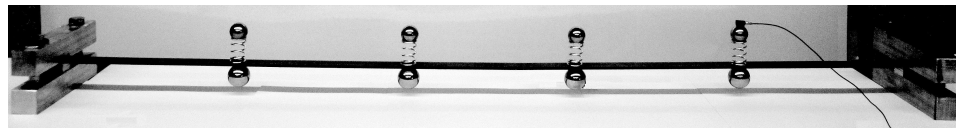
(d) Asymmetric two-fold periodicity

Figure 3.4: Experimental arrangements for four cases.

smaller range of bandwidth. An ideal hit from the impulse hammer ensures that there are no multiple hits. Because the impulse signal exists for a short period of time, a pre-trigger delay is employed. This ensures that the impulse and the response signals prior to the impulse are also captured. In other words, the entire signal is obtained. A typical impulse and the corresponding time response is shown in Fig 3.6. It can be seen that the impulse is clean with no multiple hits and is of a very short duration.

A Fast Fourier Transform (FFT) of the time response signal is then performed. This converts the time domain signal into the frequency domain. Thereafter, a transfer function is performed on the signal which yields the acceleration to force response of the impulse (FRF). This FRF is checked for coherence. Coherence is a reflection of the quality of the obtained signal. It quantifies the correlation of the output to the input. Coherence function of a measurement is given by

Input through impulse hammer, output from accelerometer

Signal Conditioner

Post processing in MATLAB

BNC
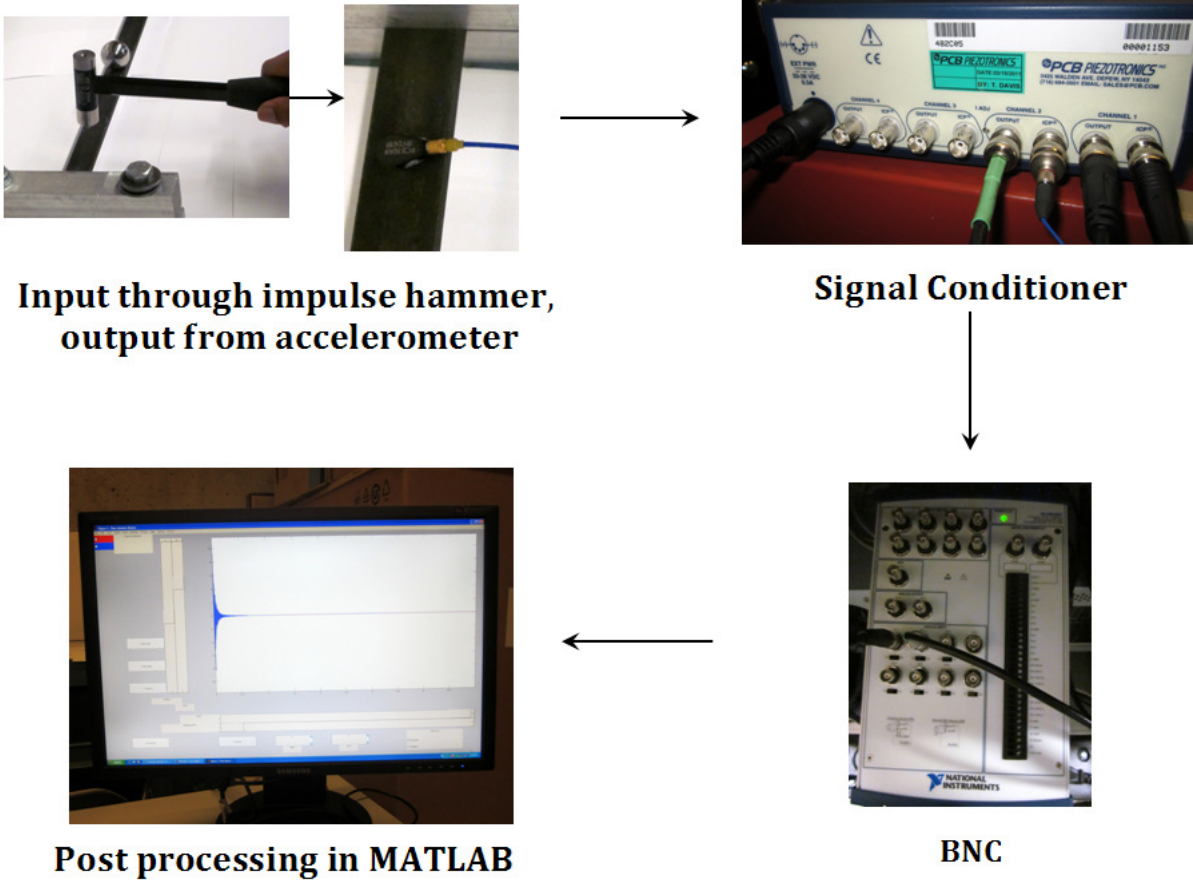
Figure 3.5: Sequence of operations for performing modal analysis.

$\gamma^2(\omega) = \dfrac{|S_{xy}(\omega)|^2}{S_{xx}(\omega)S_{yy}(\omega)}$, S_{xx} is the auto correlation of the input, S_{yy} is the auto correlation of the output and S_{xy} is the cross correlation of the input and output. A coherence value of 1 or 0 on the log scale is ideally desired. This indicates that the frequency response obtained is due to the impulse and is uncontaminated by noise. A coherence versus frequency plot is shown in Fig 3.7. Impulse is given close to the left end of the beam and the transfer FRF is measured at the right end using the accelerometer. The linear response transfer FRF of the acceleration to the impulse force for the beam is obtained, the natural frequencies, and damping parameters can then be identified. In order to further eliminate noise, averages of
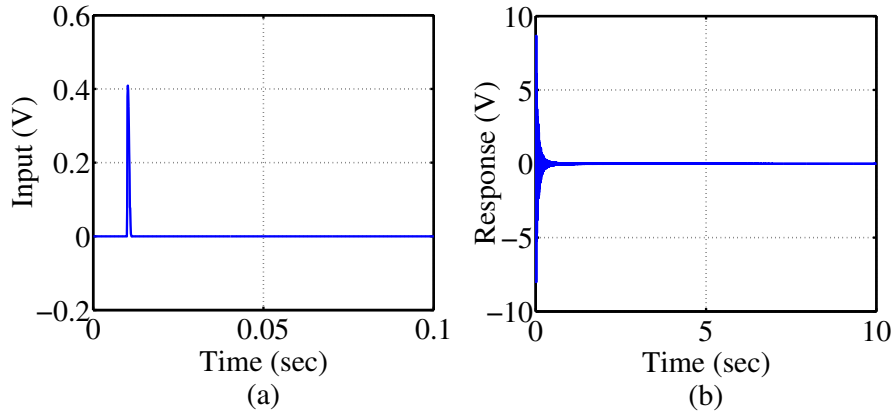
Figure 3.6: Impulse hammer and the corresponding time response data. (a)
Impulse Hammer data and (b) Time response plot

several power spectra are considered. This is done by averaging multiple impulse
test responses. For our purposes, we repeated the impulse test four times to obtain
the averaged FRF over four measurements.
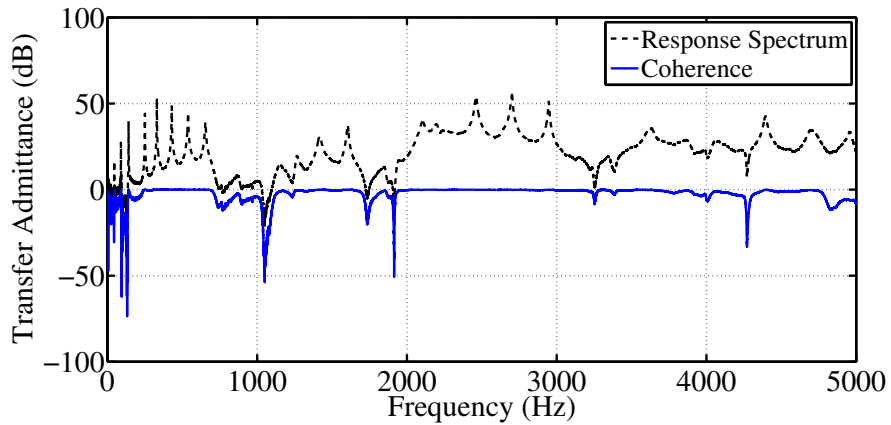
Figure 3.7: Frequency response plot with coherence function. The coherence
shows a value close to zero over the range of frequencies indicating that
the spectrum obtained is clean, without noise.

For our experimental set-up, an impulse is delivered to the beam by means of
an impulse hammer at its one end. The hammer is a PCB type, with a sensitivity

of 11.2 mV/N. The system is excited by means of a metal tip. An accelerometer, PCB 352A24 with a sensitivity of 10.2 $\frac{mV}{m/s^2}$ placed at the other end of the beam senses the vibrations and the sensor signal is delivered to the signal conditioner. The conditioned signal is now passed through an inbuilt data acquisition system and the response is post processed in MATLAB©.

3.4   Results and Discussion

Fig 3.8 shows the linear response spectrum of the beam with attached periodic masses; Fig 3.8(a) corresponds to the Bragg frequencies and Fig 3.8(b) corresponds to the sub-Bragg frequencies. On introducing periodicity, characteristic pass and stop bands are seen. The grey shades marked in the figures correspond to the bandgaps that were calculated using FE techniques, the results of which were already presented in Chapter 2. It can be seen that the bandgaps predicted by theory are in excellent agreement with the results obtained through experiments. Thus, Bragg bandgaps are introduced and there are no sub-Bragg bandgaps for this system.

Fig 3.9 shows the linear response spectrum of a beam with periodically placed spring mass resonators. The effect of introducing resonators is to narrow the bandgaps corresponding to the Bragg frequencies. However, a sub-Bragg bandgap around the frequency corresponding to the resonant frequency of the attached resonator, 68.5 Hz is introduced. Recall that an analogy was made between the local resonant units and the concept of vibration absorbers in Section 1.2.1 The concept of a vibration absorber is to introduce an anti-resonance at a desired frequency of the main system by attacing a spring mass system whose resonant frequency is the frequency at which an anti-resonance is desired. It is known [76] that the effect of attaching an absorber to a main mass is to produce an anti-resonance at the desired frequency while introducing two new resonances at frequencies away from the target frequency. Fig 3.9(b) shows the same result experimentally as well.

Fig 3.10 shows the linear response spectrum of a beam with symmetric two-fold periodicity. The effect of two fold periodicity on the beam is to open up the bandgaps corresponding to the Bragg frequencies, while preserving the local resonant bandgap. Note that the width of the gap is smaller than in the former case,

owing to a reduction in the mass ratio of the absorber to the beam. Here, a two-fold periodicity increases the total mass of the beam. Thus the ratio of the mass of the resonator to that of the beam is now decreased as compared to the case with a beam with attached resonators. It has been shown in Section 2.5, that a decreased mass ratio narrows the width of the bandgap (See Fig 2.17). Here, the stiffness of the resonators has been maintained a constant.

Fig 3.11 shows the linear response spectrum of a beam with asymmetric two-fold periodicity. The masses on the beam are greater, causing a widening of the gaps corresponding to the Bragg frequencies, while the sub-Bragg bandgap narrows further owing to a decreased mass ratio.
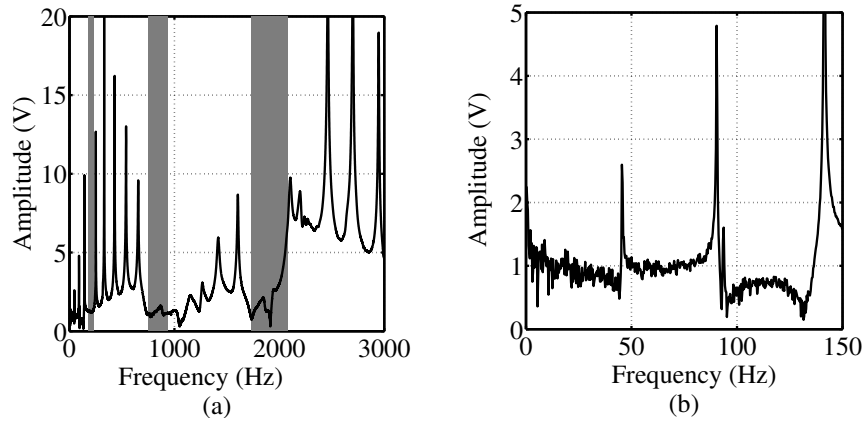
Figure 3.8: Linear response spectrum of a beam with periodically placed masses. (a) Bragg frequencies (b) Sub-Bragg frequencies. The grey shades correspond to the bandgaps, calculated analytically. While Bragg bandgaps exist, there are no sub-Bragg bandgaps.

3.5 Conclusions

In this chapter, experiments have been conducted to verify the bandgap formation for various types of periodicity, which were obtained via FE techniques in Chapter 2. To this end, we first corroborated our theoretical model by comparing the natural frequencies obtained through finite element technique in MATLAB© with a robust FE package, ABAQUS©. We found that the natural frequencies for the first 20 modes are in excellent agreement.
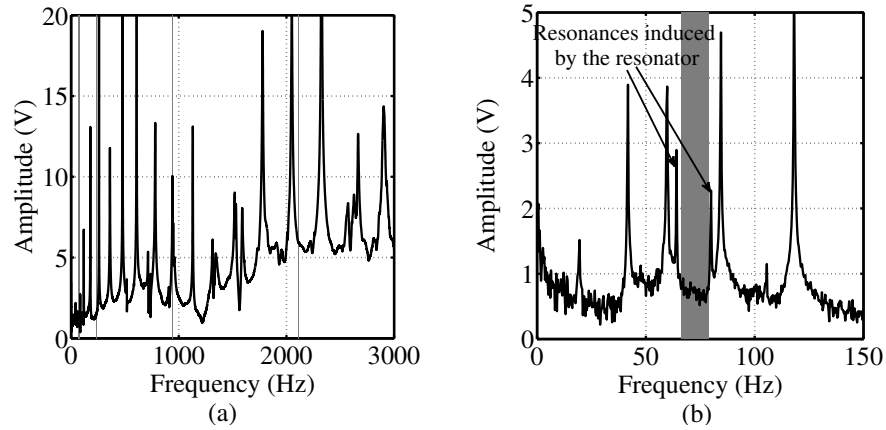
Figure 3.9: Linear response spectrum of a beam with periodically placed resonators. (a) Bragg frequencies, (b) Sub-Bragg frequencies. The grey shades correspond to the bandgaps, calculated analytically. While Bragg bandgaps cease to exist, there is a sub-Bragg bandgap at the resonant frequency of the absorber, 68.5 Hz.
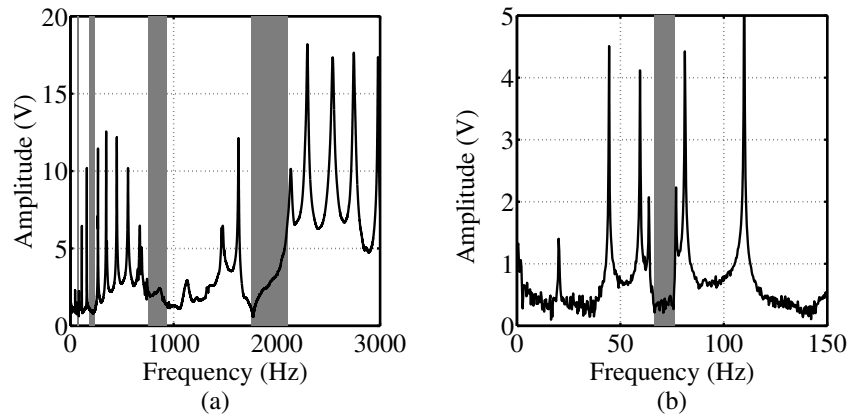
Figure 3.10: Linear response spectrum of a beam with symmetric two fold periodically placed resonators and masses. (a) Bragg frequencies (b) Sub-Bragg frequencies. The grey shades correspond to the bandgaps, calculated analytically. While Bragg band gaps open up, there is a sub-Bragg bandgap at the resonant frequency of the absorber, 68.5 Hz.

Experiments included impulse tests on a low-carbon steel beam of finite length with fixed end conditions. Four sets of experiments were performed. The first

56
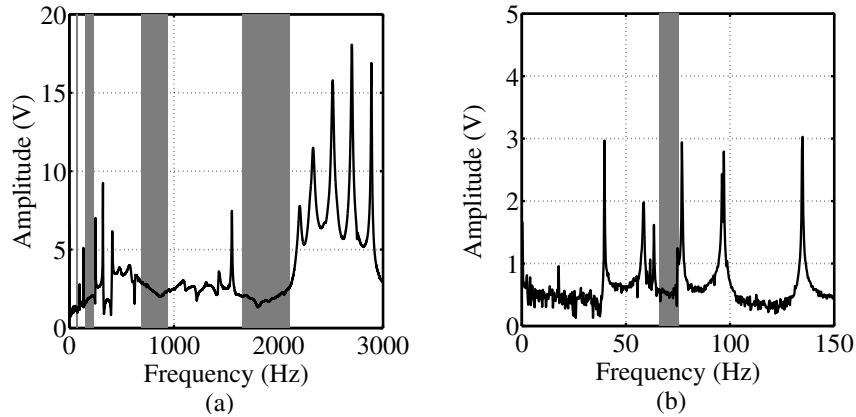
Figure 3.11: Linear response spectrum of a beam with asymmetric two-fold periodically placed resonators and masses.(a) Bragg frequencies (b) Sub-Bragg frequencies. The grey shades correspond to the bandgaps, calculated analytically. Bragg bandgaps are now wider than in the symmetric two-fold periodicity case. There is a sub-Bragg bandgap at the resonant frequency of the absorber, 68.5 Hz.

was a fixed beam with periodically placed masses. the second was a fixed beam with periodically placed resonators. The third was a fixed beam with a symmetric two-fold periodicity and the last was a fixed beam with an asymmetric two-fold periodicity.

The following results were found, which are in agreement with our theoretical predictions. We found that periodically placed masses produce bandgaps at the Bragg frequencies. These gaps increase with increasing frequency due to reduced modal coupling. With periodically placed absorbers, the bandgaps related to Bragg frequencies narrow down and open a bandgap at the resonant frequency of the resonator corresponding to sub-Bragg frequencies. A symmetric two-fold periodic system produces a bandgap at the sub-Bragg frequency corresponding to the resonant frequency of the absorber while opening up the bandgaps related to the Bragg frequencies due to periodic masses on the beam. An asymmetric two-fold periodicity helps in tailoring the bandgaps corresponding to Bragg frequencies while preserving the local resonant bandgap.

Chapter 4

Localized Response Due to Disorder and Nonlinearity

Systems studied thus far in this thesis were perfectly periodic, operating in linear response regime. Localization can also result from the presence of distributed defects and nonlinearity. With a view to understanding the localization in periodic systems, we consider a two degree of freedom lumped parameter model. This model brings forth the complex interplay between disorder and nonlinearity.

4.1   Introduction

Man-made periodic structures inherently possess defects in them. It is known that a small disorder in a periodic structure causes the phenomenon of localization [16, 19, 45]. Nonlinearities often arise due to large deformations of the structure inducing geometric nonlinearities or due to material nonlinearities. Nonlinearities in periodic structures can have significant effects on the localization phenomenon. If nonlinearity is known to aid localization, it would cause the confinement of vibrations and inducing large deformations and localized stresses in structures and damage them. On the other hand, localizations induced by nonlinearities at a micro scale level might prove useful as highly sensitive regions, which may aid in sensing applications. There have been contradicting results, both from theory and experiments [8, 59], with regards to the effect of nonlinearity on localization. It is

therefore required that a thorough analysis on the effects of nonlinearity on localization be made.

A two degree of freedom system offers the possibility of studying the influence of nonlinearity coupled with various system parameters such as disorder, coupling, damping etc. on localization without entailing the difficulties associated with complex structures. A system of coupled pendula has been considered by Tjavaras et al. [51]. They showed that this simple system exhibits localization as long as the forces applied are sufficiently small such that the angles traversed by the pendula are small. On increasing the force amplitude or, in other words, on introducing nonlinearity, they concluded that localization is greatly reduced. Vakakis [77] introduced the concept of nonlinear normal modes for explaining the response of a two degree of freedom system under high degree of nonlinearity. Nonlinearity in coupled oscillators has also been studied by Aronson et al. [78]. However they studied a system of coupled oscillators assuming that they are not identical i.e. their system considered coupled pendula whose natural frequencies differed. They were interested in studying the difference of the natural frequencies on the amplitude of the output of the coupled system. A similar approach was taken up by Kuske and Erneux [79]. They found that for certain parameter regimes, stable localized solutions exist for which the amplitude of one oscillator is an order of magnitude smaller than the other. However, for our purposes, we are interested in a system of oscillators which are identical to each other. We then introduce a disorder which slightly breaks the symmetry in the system and study the effect of this disorder on the vibration amplitudes of the system.

It is common in engineering practice to plot eigenvalues against some system changing parameter such as stiffness, mass etc. On increasing either the mass, stiffness or damping, veering of natural frequencies of coupled oscillators occurs i.e. the variable parameter causes an increase/decrease in both the natural frequencies of the system and thereby induces veering. In such cases, the eigenvalues of closely related systems may either cross each other or approach each other and thereafter veer away. This phenomenon is known as eigenvalue loci veering. Crossing of the eigenvalues occurs when there is perfect symmetry in the system. This would allow for the eigenvalues of the component unitcells to be equal and the corresponding eigenvectors to exist independently. Any divergence from symmetry causes the

eigenvalues to repel each other and this causes the phenomenon of veering. A rapid rotation of eigenvectors is also noted around the region of veering as observed in [80]. Similar effects were observed for a system under small levels of damping. The phenomenon was observed experimentally in [55] for the first time. The practical application of this phenomenon is to make use of the region of veering for sensing applications of small perturbations. Perkins and Mote[81] provided a criteria for a system's eigenvalues to avoid crossing and instead veer away from each other, based on the strength of coupling. They also concluded that veering can take place in both discrete and continuous systems. Pierre[52] conducted studies on a coupled pendula model and concluded that localization and veering were different manifestations of the same phenomenon. This conclusion has come under criticism by Chen and Ginsberg [82] who concluded that veering exists even when localization is not observed. A similar conclusion was drawn by Stephen [83] who concluded that veering always occurs for a finite, non-zero coupling and not just under a weak coupling. Several approaches to the identification of veering have been provided by various authors in the past. The most common among them is the approach that involves the detection of veering by means of the eigenvalue and eigenvector derivatives employed in [84]. Stephen [83] identified the loci of the eigenvalues to be hyperbolas and the geometries of the hyberbolas and the sensitivities of the foci and asymptotes were used to detect veering. The present chapter however, does not quantify the occurrence of veering but only analyses localization as a phenomenon resulting from veering.

In this chapter, the influence of disorder on localization is studied for a two degree of freedom system. The system considered is a three spring two mass system as shown in Fig 4.1. Localization in the context of veering is studied. It is shown that mode sensitivity or swapping occurs only under the case of weak coupling, indicating veering. Localization is also observed only under this condition thus confirming that both these phenomena are more predominant under similar conditions.

The organization of this chapter is as follows: In Section 4.2, linear analysis is performed on a two degree of freedom spring mass system. Veering in the context of localization is pursued. Analytical relations between the disorder, coupling and the degree of localization in the system are derived. Thereafter in Section 4.3, small

60

nonlinearity is introduced in the system. Cubic nonlinearity in the ground springs is assumed while the coupling spring is maintained linear. Analytical solutions are presented which were obtained using a one-term harmonic balance method. Solutions obtained analytically are compared with numerical results obtained using fourth-order Runge-Kutta method. Subsequently, a small value of damping is introduced in the system and the effect of damping on localization is presented in Section 4.4. The chapter concludes with a discussion of the key results in Section 4.5.

4.2 Linear Analysis
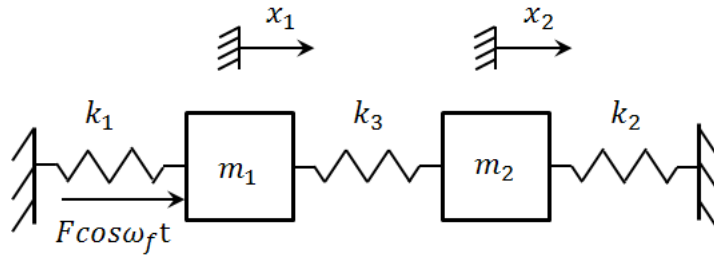
Figure 4.1: A two-degree of freedom spring-mass system

A simple two degree of freedom system such as the one shown in Fig 4.1 is considered. Firstly we assume that the system is unforced. The energy expression for this system may then be written as:

$$
\begin{aligned}
KE &= T \\
&= \frac{1}{2}m_1\dot{x}_1^2 + \frac{1}{2}m_2\dot{x}_2^2,
\end{aligned}
\tag{4.1}
$$

$$
\begin{aligned}
PE &= V \\
&= \frac{1}{2}k_1 x_1^2 + \frac{1}{2}k_3(x_2 - x_1)^2 + \frac{1}{2}k_2 x_2^2,
\end{aligned}
\tag{4.2}
$$

$$
\mathscr{L} = T - V \text{ (Lagrangian).}
\tag{4.3}
$$

The Euler-Lagrange equations of motion are

$$\frac{d}{dt}\left[\frac{\partial \mathcal{L}}{\partial \dot{x}_1}\right] - \frac{\partial \mathcal{L}}{\partial x_1} = 0,$$

$$\frac{d}{dt}\left[\frac{\partial \mathcal{L}}{\partial \dot{x}_2}\right] - \frac{\partial \mathcal{L}}{\partial x_2} = 0 \tag{4.4}$$

from which we obtain the governing equations of motion as:

$$m_1 \ddot{x}_1 + (k_1 + k_3)x_1 - k_3 x_2 = 0,$$

$$(1+D)m_1 \ddot{x}_2 + (k_2 + k_3)x_2 - k_3 x_1 = 0 \tag{4.5}$$

We now proceed to systematically non-dimensionalize the system. For a symmetric case, $m_1 = m_2 = m$ and $k_1 = k_2 = k$. Disorder in the system can be thought of as a breaking of this symmetry which could be brought about by either varying either the masses or the stiffnesses. Let disorder in the system be represented by 'D' and assume that the disorder is in the second mass and is additive in nature, such that $m_2 = m_1(1+D)$.

$$\frac{m}{k}\ddot{x}_1 + (1 + \frac{k_3}{k})x_1 - \frac{k_3}{k}x_2 = 0,$$

$$\frac{(1+D)m}{k}\ddot{x}_2 + (1 + \frac{k_3}{k})x_2 - \frac{k_3}{k}x_1 = 0 \tag{4.6}$$

Introducing a non-dimensional time $\tau = \omega t$ where, $\omega = \sqrt{\frac{k}{m}}$, we can write the following equations:

$$\frac{d}{dt} = \frac{d}{d\tau}\frac{d\tau}{dt} = \omega\frac{d}{d\tau};$$

$$\frac{d^2}{dt^2} = \omega^2\frac{d^2}{d\tau^2}.$$

Therefore equations in (4.6) reduce to

$$\omega^{-2}\ddot{x}_1 + (C+1)x_1 - Cx_2 = 0,$$

$$(1+D)\omega^{-2}\ddot{x}_2 + (C+1)x_2 - Cx_1 = 0, \tag{4.7}$$

where C is the non dimensional coupling parameter, $\dfrac{k_3}{k}$. The re-scaled matrix equation can therefore be written as:

$$
\begin{bmatrix} \omega^{-2} & 0 \\ 0 & (1+D)\omega^{-2} \end{bmatrix} \begin{bmatrix} \ddot{x}_1 \\ \ddot{x}_2 \end{bmatrix} + \begin{bmatrix} 1+C & -C \\ -C & 1+C \end{bmatrix} \begin{bmatrix} x_1 \\ x_2 \end{bmatrix} = \begin{bmatrix} 0 \\ 0 \end{bmatrix} \tag{4.8}
$$

The steady state response of the system can be written as $x_1 = X_1 cos\omega t$ and $x_2 = X_2 cos\omega t$. Therefore,

$$
\begin{bmatrix} 1+C-\omega_f^2\omega^{-2} & -C \\ -C & 1+C-(1+D)\omega^2\omega^{-2} \end{bmatrix} \begin{bmatrix} X_1 \\ X_2 \end{bmatrix} = \begin{bmatrix} 0 \\ 0 \end{bmatrix} \tag{4.9}
$$

The Eigenvalues, $\lambda = \omega^2$, plotted against the disorder for the cases of weak and strong coupling are shown in Fig 4.2 and 4.3. Fig 4.2 corresponds to the case of non-dimensional weak coupling of a value of 0.01. Fig 4.3 corresponds to the case of strong coupling with a non-dimensional coupling value ten times that of the previous case. In all these figures, the dotted curve corresponds to the out of phase motion and the solid curve corresponds to the in-phase motion. Corresponding Eigenvector diagrams are plotted for various levels of disorder. The eigenvectors are shown in the inset. The amplitudes of the eigenvectors on the axes are indicative of the amount of displacements in both the oscillators. The intercepts of the rotating vectors indicate the amplitudes of steady vibrations in the corresponding natural mode of each of the masses. It is evident that the eigenvalues associated with each mass exhibits greater veering for the case of weak coupling as compared to the case of strong coupling. Decreasing the coupling further would induce a greater radius of curvature at the zone of veering. Additionally, the intercepts of the corresponding rotating vectors display a greater localization of displacements to the first mass for a 5% disorder in the system for the case of weak coupling, as can be seen from the intercepts of the vectors on the axes. No such confinement of displacements to the first mass is seen in Fig 4.3 , wherein the intercepts of the rotating vectors exhibit nearly equal displacements for both masses, regardless of the level of disorder when the coupling strength is high. Also, it can be seen from the rotating vector diagrams that the mode shapes undergo a *'switching'* effect as the eigenvalues pass through the zero disorder line in Fig 4.2. Negligible effects are observed in the case of strong coupling. This shows that weak coupling coupled

63
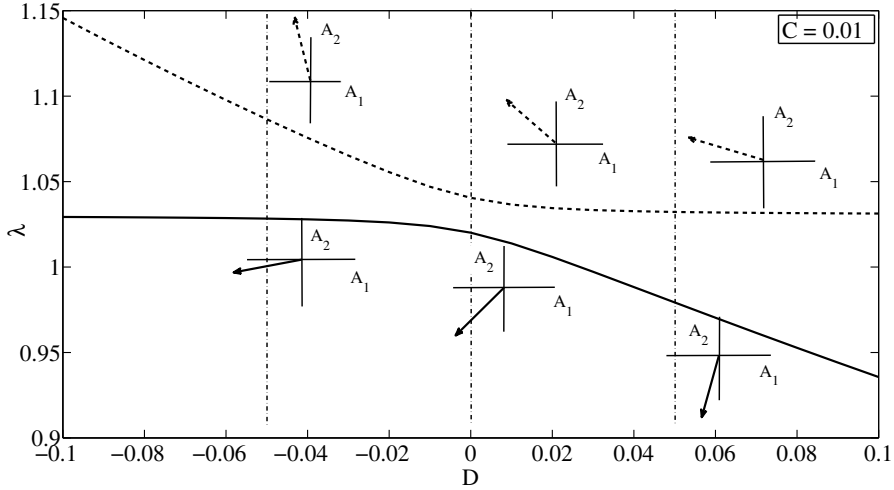
Figure 4.2: Eigenvalues, λ versus disorder, D for weak couping C=0.01 with corresponding Eigenvector directions.
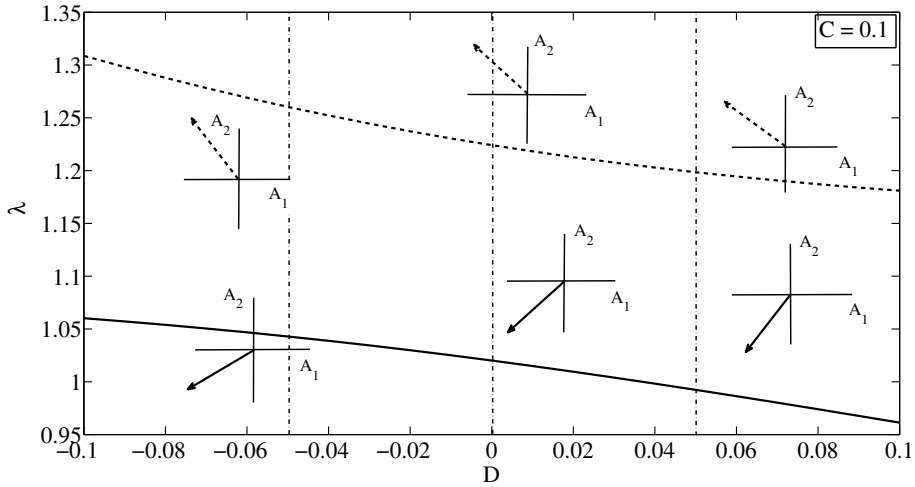

Figure 4.3: Eigenvalues, λ versus disorder, D for strong coupling C=0.1 with corresponding Eigenvector directions.

with disorder produces veering as well as confinement of energies. It can therefore be concluded that both veering and localization effects are predominant in the case

of weak coupling alone. Small perturbations in the symmetry of the system induces greater localization and rotation of the mode shapes at the vicinity of veering.

Let the system considered in Fig 4.1 be subjected to a harmonic force, such that the force is applied to the first mass. The forcing frequency is assumed to be very close to the resonant frequency of the system as we intend to study the system's localization effects of its linear modes. The matrix form of the equations shown in Eq (4.9) can then be written as:

$$\begin{bmatrix} 1 + C - \omega_f^2 \omega^{-2} & -C \\ -C & 1 + C - (1+D)\omega_f^2 \omega^{-2} \end{bmatrix} \begin{bmatrix} X_1 \\ X_2 \end{bmatrix} = \begin{bmatrix} F\cos\omega_f t \\ 0 \end{bmatrix} \qquad (4.10)$$

$$\Rightarrow X_1 = \frac{1 + C - (1+D)\omega_f^2 \omega^{-2}}{\Delta} f\cos\omega_f t;$$

$$X_2 = \frac{C}{\Delta} F\cos\omega_f t \qquad (4.11)$$

where, $\Delta = (1 + C - (1+D)\omega_f^2)(1 + C - \omega_f^2) - C^2$, represents the determinant.

Localization Ratio γ can be defined as the ratio of the displacement of the second mass to that of the first mass. If this ratio is large, it indicates that more energy is propagated from the first mass to the second mass suggesting that there is no localization of energy. Similarly, a small value of the localization ratio implies that there is a strong localization of energy to the first mass, on force being applied to the first mass. Therefore,

$$\gamma = \frac{X_2}{X_1} = \frac{C}{1 + C - (1+D)\omega_f^2 \omega^{-2}} \qquad (4.12)$$

If $\omega_f \simeq \omega$,

$$|\gamma| \simeq |\frac{C}{(C-D)}| \qquad (4.13)$$

65

Thus, for a mass disorder such that $m_2 = (1+D)m_1$, a singularity occurs when $C = D$, as can be seen in Fig 4.4. A singularity for this system means that when the first mass is subjected to a force, the displacement of the first mass is tending to zero. This can be understood by studying Eq (4.11). This equation reveals that on having disorder equal to the coupling, the value of X_1 goes to zero, while the value of X_2 is not affected by change in the coupling. This suggests that on having high values of γ, the first mass is not moving. The coupling spring ensures that the second mass moves, but the amplitude through which this mass moves cannot be infinite as the second oscillator has a finite mass associated with it. Thus, the ratio of X_2 to X_1 goes to infinity for $D = C$. Similar singularities may be defined for the various types of disorder.
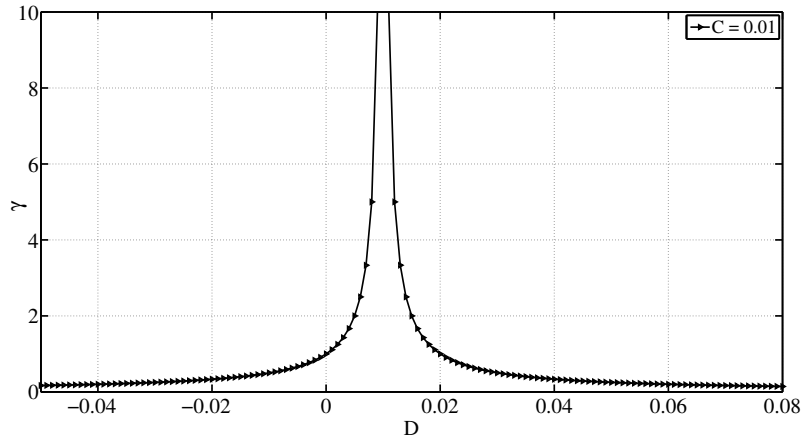
Figure 4.4: Singularity observed for $D = C$ when the disorder in the system is defined as $m_2 = (1+D)m_1$

For the case when $m_2 = (1-D)m_1$,

$$|\gamma| \simeq |\frac{1}{(C+D)}| \tag{4.14}$$

For this kind of disorder, there is a singularity only when $D = -C$, as can be seen in Fig 4.5.

When disorder in the mass is defined such that $m_2 = m_1 D$ and $k_1 = k_2$,

$$|\gamma| \simeq |\frac{C}{1+(C-D)}| \tag{4.15}$$

A singularity occurs when $D = 1 + C$ or $\frac{D}{C} = 1 + \frac{1}{C}$ as shown in Fig 4.6. Here, a coupling value of 0.01 was considered.
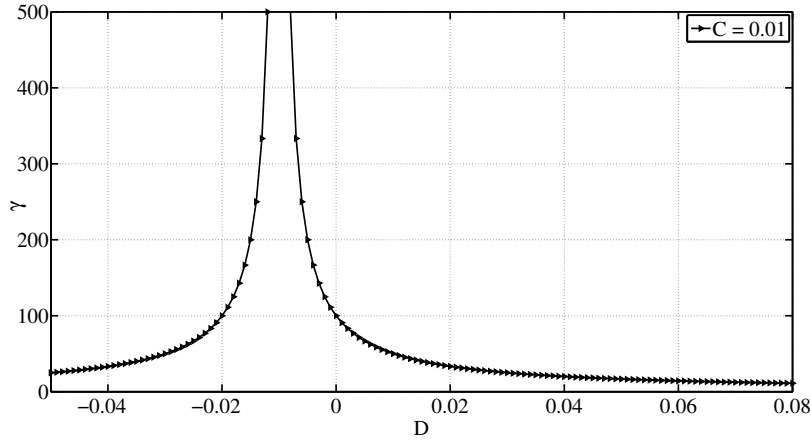
Figure 4.5: A singularity is observed at $D = -C$ when the disorder in the system is defined as $m_2 = (1-D)m_1$

Assuming that the disorder is now defined in terms of the stiffness in the springs, such that $m_1 = m_2 = m$ and $k_3 = k_1(1 \pm D)$,

$$|\gamma| \simeq |\frac{C}{(C \pm D)}| \tag{4.16}$$

For such a definition of the disorder, a singularity occurs at $C = D$ when $k_2 = k_1(1-D)$ and at $C = -D$ when $k_2 = k_1(1+D)$

When disorder in the stiffness is defined such that $k_2 = k_1 D$ and $m_1 = m_2$,

$$|\gamma| \simeq |\frac{C}{(C+D)-1}| \tag{4.17}$$

67
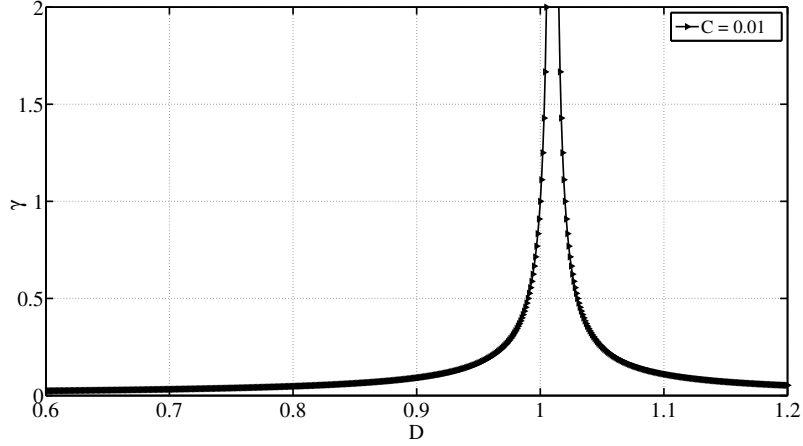
Figure 4.6: Singularity observed for $D = 1 + C$ when the disorder in the system is defined as $m_2 = Dm_1$. Here, $C = 0.01$.

A singularity occurs when $D = 1 - C$. Thus, it is evident that the occurrence of singularities depends on the way the disorder is introduced in the system. The values to the left of the singularity represents a region of low disorder. The region to the right of the singularity represents a region of high disorder. It can be seen that the region showing low disorder shows low localization and the region exhibiting high disorder shows a region of high localization. The regions at low disorder have a high coupling associated with them and higher the coupling, lower is the localization. As one moves deeper into the regions on the right, we move to higher and higher levels of disorder such that disorder now dominates the coupling and the system is now greatly localized.

For the disorder defined to be additive in the second mass, instead of choosing the forcing frequency to be equal to the first resonant frequency of the system, we now choose a forcing frequency value that is lesser than the natural frequency of the system. We see that the effect is to push the point of singularity towards higher disorder. The explanation for this can be once again given by observing the Eq (4.11). It may be observed that X_1 is a value that depends on the forcing frequency. On decreasing the forcing frequency, a greater value of disorder must be induced
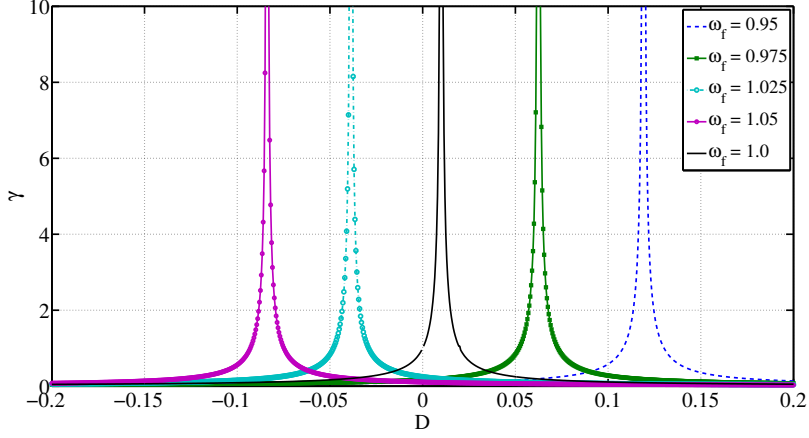
Figure 4.7: Influence of forcing frequency on localization ratio. Decreasing the forcing frequency pushes the singularity to the right while increasing the forcing frequency pushes the singularity to the left.

in order for the singularity to occur. Thus the singularity moves to the right. The corresponding graph depicting the same is shown in Fig 4.7.

4.3 Effect of Nonlinearity

If the springs k_1 and k_2 in Fig 4.1 were made cubic nonlinear, the equations of motion for the system could be written as:

$$\ddot{x}_1 + x_1 + C(x_1 - x_2) + \alpha x_1^3 = F\cos\omega_f t$$
$$(1+D)\ddot{x}_2 + x_1 + C(x_2 - x_1) + \alpha x_2^3 = 0, \tag{4.18}$$

where α represents the coefficient of the cubic nonlinear spring. The α values are maintained the same in both the springs so as to maintain symmetry as we wish to understand the effects of nonlinearity in itself on the localization phenomenon. When one encounters nonlinearity with respect to the spring such that the force which causes the spring to elongate increases at a slower rate than the elongation, such a spring is a *'softening spring'*. On the other hand, if the force increases at

a faster rate than the elongation, such a spring is called a *'hardening spring'*. A positive value of α implies that the spring is hardening in nature and a negative value of α corresponds to a softening spring.

As a first approximation, let x_1 and x_2 be represented by $X_1 \cos\omega t$ and $X_2 \cos\omega t$ respectively, where the amplitudes X_1 and X_2 are unknowns. By making such an assumption, we are assuming that the nonlinearities in the system are small. Heavy nonlinearities would push the system into chaos such that the system does not exhibit periodic motions. In other words, on maintaining small nonlinearities, the system is constrained to Limit Cycle Oscillations. Higher values of α will subject the system to motions which are not periodic. Thus our work is restricted to the study of the influence of small nonlinearities.

The above equations can be written as:

$$-\omega^2 X_1 \cos\omega t + X_1 \cos\omega t + C(X_1 - X_2)\cos\omega t + \alpha(X_1 \cos\omega t)^3 = F\cos\omega_f t,$$

$$-(1+D)\omega^2 X_2 \cos\omega t + X_2 \cos\omega t + C(X_2 - X_1)\cos\omega t + \alpha(X_2 \cos\omega t)^3 = 0 \quad (4.19)$$

Using the identity

$$\cos 3\omega t = \frac{3}{4}\cos\omega t + \frac{1}{4}\cos 3\omega t, \quad (4.20)$$

Eq (4.19) can be expressed as:

$$-\omega^2 X_1 \cos\omega t + X_1 \cos\omega t + C(X_1 - X_2)\cos\omega t +$$
$$\alpha(X_1^3)(\frac{3}{4}\cos\omega t + \frac{1}{4}\cos 3\omega t) = f\cos\omega_f t,$$
$$-(1+D)\omega^2 X_2 \cos\omega t + X_2 \cos\omega t + C(X_2 - X_1)\cos\omega t +$$
$$\alpha(X_2^3)(\frac{3}{4}\cos\omega t + \frac{1}{4}\cos 3\omega t) = 0 \quad (4.21)$$

Balancing the terms containing $\cos\omega t$ and ignoring the $\cos 3\omega t$ term,

$$-\omega^2 X_1 + X_1 + C(X_1 - X_2) + \frac{3}{4}\alpha(X_1)^3 = f$$

$$-(1+D)\omega^2 X_2 + X_2 + C(X_2 - X_1) + \frac{3}{4}\alpha(X_2)^3 = 0 \qquad (4.22)$$

Writing X_2 in terms of X_1 we obtain a polynomial in X_1 whose coefficients are:

$$\begin{aligned}
&[81\alpha^4, 0, 324\alpha^3 C + 324\alpha^3 - 324\alpha^3\omega^2 - 324D\alpha^3\omega^2, 0, 432D^2\alpha^2\omega^4 \\
&- 864D\alpha^2 C\omega^2 + 864D\alpha^2\omega^4 - 864D\alpha^2\omega^2 + 432\alpha^2 C^2 - 864\alpha^2 C\omega^2 + \\
&864\alpha^2 C + 432\alpha^2\omega^4 - 864\alpha^2\omega^2 + 432\alpha^2, 0, -192\alpha D^3\omega^6 + 576\alpha D^2 C\omega^4 \\
&- 576\alpha D^2\omega^6 + 576\alpha D^2\omega^4 - 576\alpha DC^2\omega^2 + 1152\alpha DC\omega^4 - 1152\alpha DC\omega^2 \\
&- 576\alpha D\omega^6 + 1152\alpha D\omega^4 - 576\alpha D\omega^2 + 384\alpha C^3 - 768\alpha C^2\omega^2 + 768\alpha C^2 \\
&+ 576\alpha C\omega^4 - 1152\alpha C\omega^2 + 576\alpha C - 192\alpha\omega^6 + 576\alpha\omega^4 - 576\alpha\omega^2 \\
&+ 192\alpha, 0, 256C^2 + 512C^3 - 512C^2\omega^2 - 512C^3\omega^2 + 256C^2\omega^4 - 256DC^2\omega^2 \\
&- 256DC^3\omega^2 + 256DC^2\omega^4, 256FC^3] \quad (4.23)
\end{aligned}$$

Solving the above polynomial for X_1 and solving similarly for X_2 yields the analytical solution for the localization ratio γ which is $\frac{X_2}{X_1}$. We consider small nonlinear coefficient values (α) in the range of 0 to 0.3. Fig 4.8 shows the power spectra for for two cases. Fig 4.8(a) corresponds to the power spectrum response of the first mass for an α value of 0. Similarly, Fig 4.8(b) shows the power spectrum response of the second mass when the first mass is displaced. α value is 0. Fig 4.8(c) shows the power spectrum response of the first mass when α is 0.3 and Fig 4.8(d) shows the power spectrum response of the first and second mass for α value of 0. However on introducing slight nonlinearity in the system, the occurrence of a cluster of peaks at the odd harmonics for the two masses is clear. This shows that the strength of nonlinear values we have chosen are introducing nonlinear effects in the system.

As a check for accuracy of our analytical solution, we compare the solution for γ vs disorder for varying levels of nonlinearities obtained through numerical method. Fig 4.9 shows the comparison between numerical and analytical methods

71
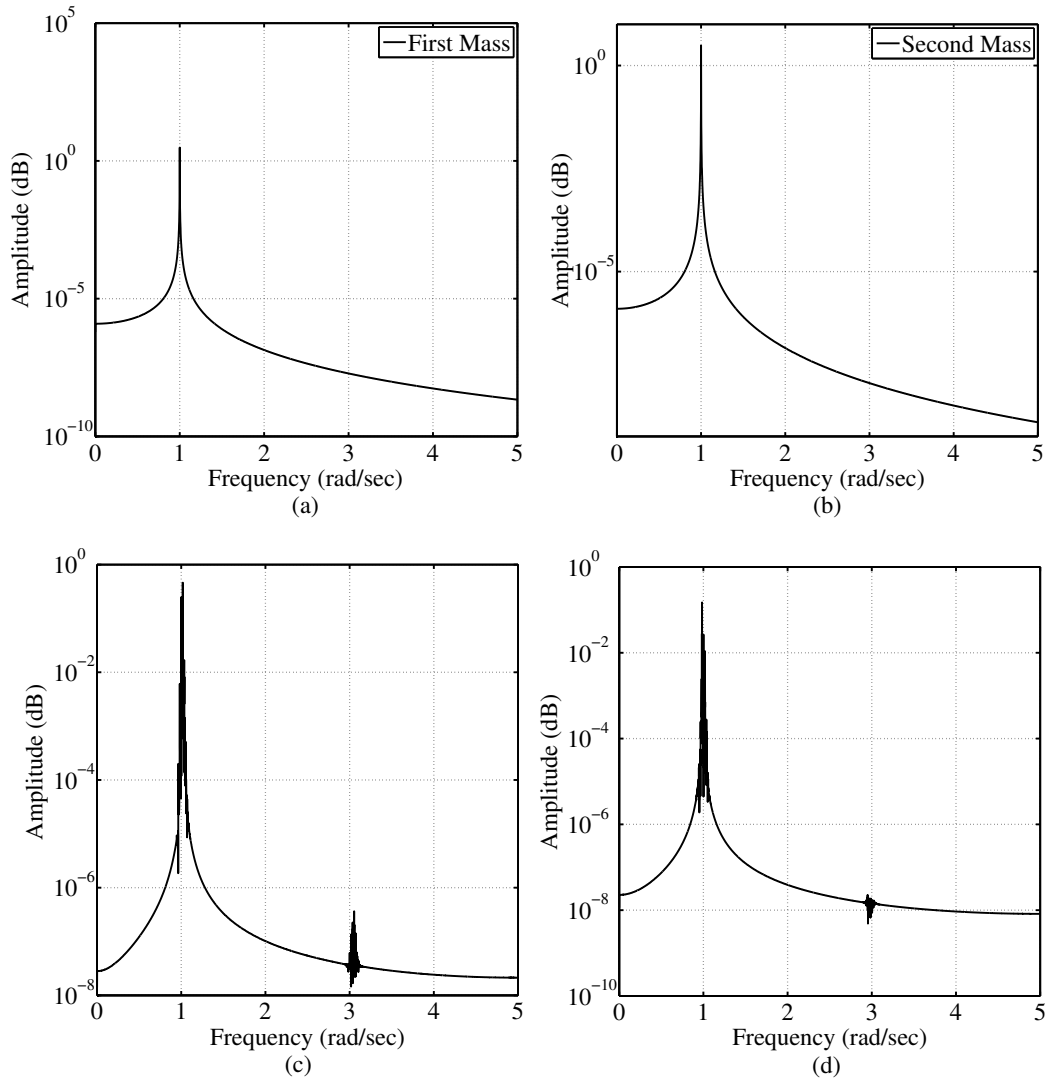
Figure 4.8: Power spectra for (a) first mass, $\alpha = 0$, (b) second mass, $\alpha = 0$ (c) first mass cubic nonlinear, $\alpha = 0.3$. (d) second for cubic nonlinear, $\alpha = 0.3$. A single peak is observed at the forcing frequency for both the masses for the linear case. Peaks are observed at the forcing frequency and the odd harmonics for the nonlinear case, indicating that the level of non linearity in the system is sufficient to bring about the nonlinear effects without setting its motion to chaos.

for four different values of nonlinearity, α ranging from 0 to 0.3. All the four plots show a reasonable comparison showing that the analytical method is reliable as long as the system exhibits a periodic response.

If we increase the coupling value C from 0.01 to twice its value as in Fig 4.11, it can be seen that a greater degree of the stiffness nonlinearity is required to induce the localizing effects for the same force amplitude. This also results in the shifting of the singularities to a higher disorder value. For a linear case, i.e. when α value is zero, the resonance peak occurs at disorder value equal to the coupling value. In other words, increasing coupling requires greater values of α as compared to the values used in 4.10 to induce localization.

Fig 4.10 shows γ for varying D values for various values of nonlinearities under a constant weak coupling value of 0.01. When α is 0, i.e. under no nonlinearity in the system, the localization ratio shows a singularity at D=C value of 0.01 as expected. As the degree of nonlinearity in the system is increased, the singularities move towards the right and ultimately converge at a linear value of 0.25 as the disorder in the system increases when the applied force amplitude is 0.001. It should however be noted that the α values considered here are small such that no chaos is being introduced in the system. Higher values of α would not yield convergence at higher disorder values.

Fig 4.12 shows γ vs D for zero, positive and negative values of α representing linear case, hardening nonlinearity and softening nonlinearity respectively. It can be seen that the effect of a hardening spring is to push the singularity towards the right, while that of the softening spring is to shift the singularity towards the left. It may be followed from the inset of Fig 4.12 that under no disorder system or in other words, under perfect symmetry in the system, nonlinearity either localizes or de-localizes the system. The effect of a hardening spring is to enhance localization in the system while that of a softening spring is weaken to it. For higher levels of disorder, the softening and hardening non linear springs behave like a linear spring. As the disorder in the system is being increased, the second mass is increasing. As the coupling in the system is maintained a constant, the regions to the right of the singularity implies regions of high disorder. This results in the disorder playing a greater role in determining localization than the stiffness (coupling) parameter.
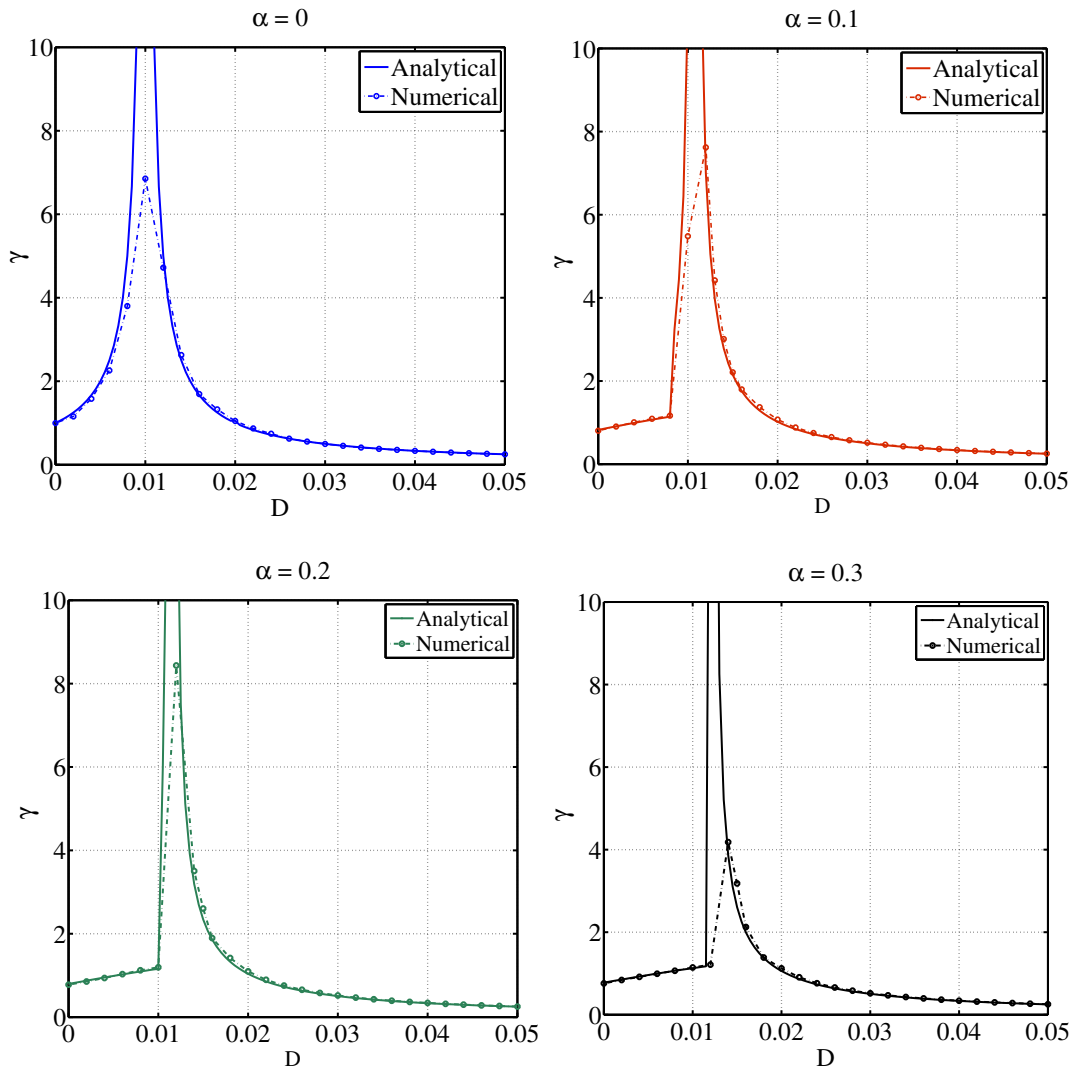
Figure 4.9: Comparison of analytical and numerical results. A comparison of the localization ratio vs disorder for values of α 0, 0.1, 0.2 and 0.3. The force amplitude for each case is 0.001 N and non-dimensional coupling is 0.01. There is excellent agreement between the two solutions.

Thus the nonlinearity which is in the stiffness (coupling) ceases to make an impact as the disorder is increasing, for small α values.
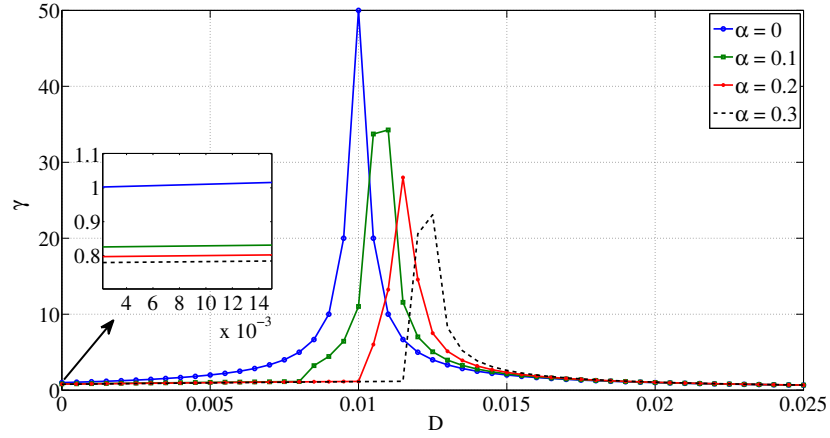
Figure 4.10: Localization ratio vs disorder for varying degrees of nonlineari-
ties obtained by analytical method for a constant value of C=0.01 and
under a harmonic force amplitude of 0.001.
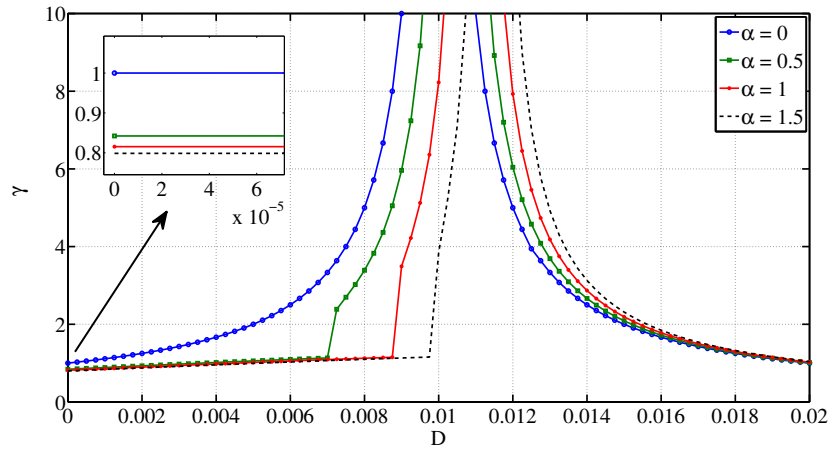
Figure 4.11: Increasing the coupling value to twice its value (0.02) reduces
localization in the system at zero disorder, as can be seen from the
inset and a greater value of nonlinearity is now required to bring any
pronounced effects.

This result also shows that even for a zero disorder system which is perfectly
symmetric, small orders of nonlinearity in itself induces a localization in it. As
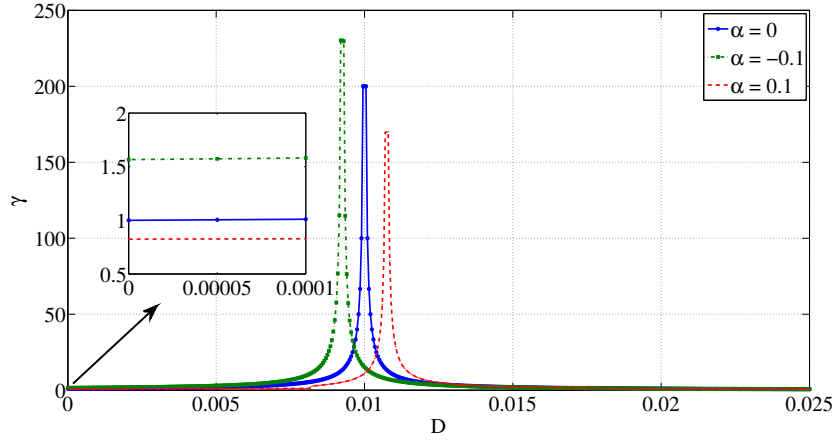
Figure 4.12: Hardening nonlinearity localizes the system while a softening nonlinearity de-localizes it when there is no disorder in the system. Inset shows the hardening softening and linear springs at zero disorder. It is evident that nonlinearity itself causes localization or de-localization in the system even at zero disorder. Region to the left of the singularity is a region wherein the hardening nonlinearity localizes the system more than the softening nonlinearity. The region to the right of the singularity, on the other hand depicts a region where the softening nonlinearity localizes the system more than the softening nonlinearity.

we increase the disorder in the system, we see that the singularities are moving towards the right or left depending on the nature of material nonlinearity and the system still behaves linearly at higher values of disorder for small nonlinearities.

On increasing the force in the system to two times its original value, the displacements of the masses increase and hence the cubic spring forces are dominant and thereby increase localization in the system. For the same values of α, the system is more sensitive to the nonlinearity and shifts the singularities further towards an increasing disorder for the same coupling value. The dotted lines in Fig 4.13 correspond to lower force while the solid lines correspond to a higher force amplitude. The inset in the figure also shows that at zero disorder, increase in the force amplitude increases the localization in the system.
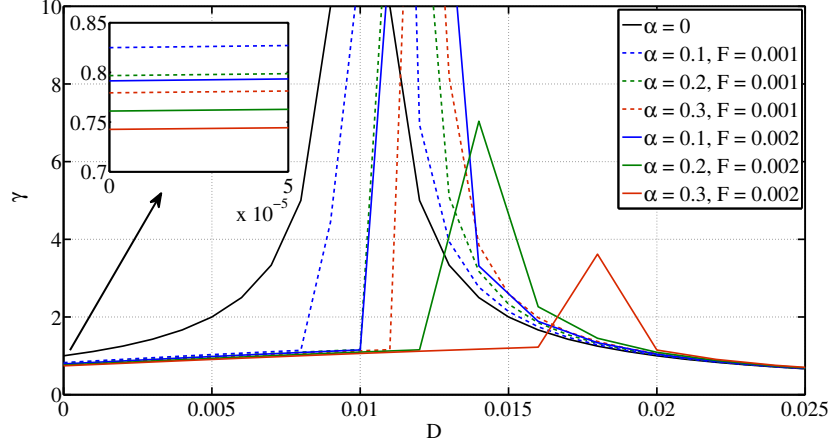
Figure 4.13: Influence of force amplitude on localization ratio. Increasing the force increases localization in the system at zero disorder, as can be seen from the inset. The additional effect is to push the singularities further to the right. The coupling value is 0.01 for both force amplitudes.

4.4 Influence of Damping

A damped two degree of freedom system is shown in Fig 4.14. On introducing damping, the system is now introduced with a sine term. This cannot be solved using harmonic balance. Therefore an alternative is to a phase shift in the damping to write the term as cosine, which is equivalent to bringing about a phase shift in the force term. We thereby introduce two components of forces f_1 and f_2. Now the equations of motion of the spring mass system can be written as:

$$\ddot{x}_1 + c\dot{x}_1 + x_1 + C(x_1 - x_2) + \alpha x_1^3 = f_1 \cos\omega_f t - f_2 \sin\omega_f t$$
$$(1+D)\ddot{x}_2 + c\dot{x}_2 + x_1 + C(x_2 - x_1) + \alpha x_2^3 = 0, \qquad (4.24)$$

where, c corresponds to the coefficient of viscous damping. Once again, we assume the system to only periodic oscillations and assume x_1 and x_2 to be represented by $X_1 \cos\omega t$ and $X_2 \cos\omega t$ respectively. By performing harmonic balance as above,
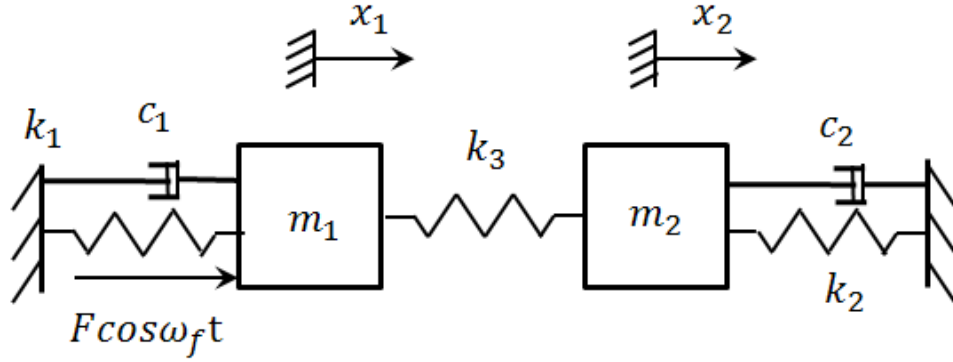
Figure 4.14: Damped two degree of freedom model.

$$-\omega^2 X_1 cos\omega t - c\omega X_1 sin\omega t + X_1 cos\omega t + \alpha(X_1 cos\omega t)^3$$
$$+C(X_1 cos\omega t - X_2 cos\omega t) = f_1 cos\omega_f t - f_2 sin\omega_f t,$$
$$-(1+D)\omega^2 X_2 cos\omega t - c\omega X_2 sin\omega t + \alpha(X_2 cos\omega t)^3$$
$$+C(X_2 cos\omega t - X_1 cos\omega t) = 0 \tag{4.25}$$

Using the identity

$$cos3\omega t = \frac{3}{4}cos\omega t + \frac{1}{4}cos3\omega t, \tag{4.26}$$

We now apply a harmonic balance of the *cos* terms and ignore $cos3\omega t$ term

$$-\omega^2 X_1 + X_1 + C(X_1 - X_2) + \frac{3}{4}\alpha(X_1)^3 = f_1,$$
$$-(1+D)\omega^2 X_2 + X_2 + C(X_2 - X_1) + \frac{3}{4}\alpha(X_2)^3 = 0 \tag{4.27}$$

A harmonic balance of the *sin* terms yields,

78

$$\omega c X_1 = f_2 \tag{4.28}$$

Therefore the equations can be re-written as:

$$-\omega^2 X_1 + X_1 + C(X_1 - X_2) + \frac{3}{4}\alpha(X_1)^3 + c\omega X_1 = f,$$
$$-(1+D)\omega^2 X_2 + X_2 + C(X_2 - X_1) + \frac{3}{4}\alpha(X_2)^3 + c\omega X_2 = 0 \tag{4.29}$$

where, $f = f_1 + f_2$

Solving the above yields a polynomial in either X_1 or X_2 which can be used to determine γ values. Fig 4.15 shows the comparison between damped and undamped cases for the spring mass system. The applied force amplitude is maintained same for the damped and undamped cases. A weak coupling value of 0.01 is preserved for both cases. Localization ratio versus varying disorder for various levels of nonlinearities is shown. The dotted lines correspond to the undamped case and the solid lines correspond to the damped case.

It is clear from the inset that at zero disorder in the system, the effect of damping is to aid localization in the system. The effect of damping is to also shift the singularities towards the right, i.e. with increasing disorder, an unamped system reaches the sigularities faster than a damped one. However, for higher values of disorder, all the curves converge to the linear value.

Fig 4.16 shows the comparison between two damped cases for varying levels of nonlinearity. It shows that increasing damping increases localization and also shifts the singularities to the right. In other words, damped structures require a greater level of disorder to show singularities in the localization ratios. The dotted lines correspond to low damping and the solid line corresponds to higher damping values.

In this section we have considered a system that has nonlinearity in the ground springs and the type of nonlinearity induced was either softening or hardening in nature.
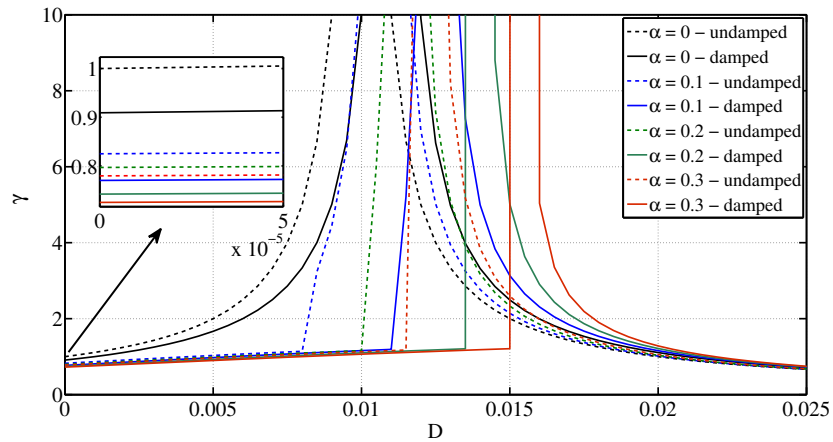
Figure 4.15: Influence of damping on localization ratio. A comparison between the damped and undamped cases is shown. The effect of damping is to aid localization for zero disorder. The force amplitude is the same in both cases (0.001 N) and the coupling is 0.01 for both the cases.
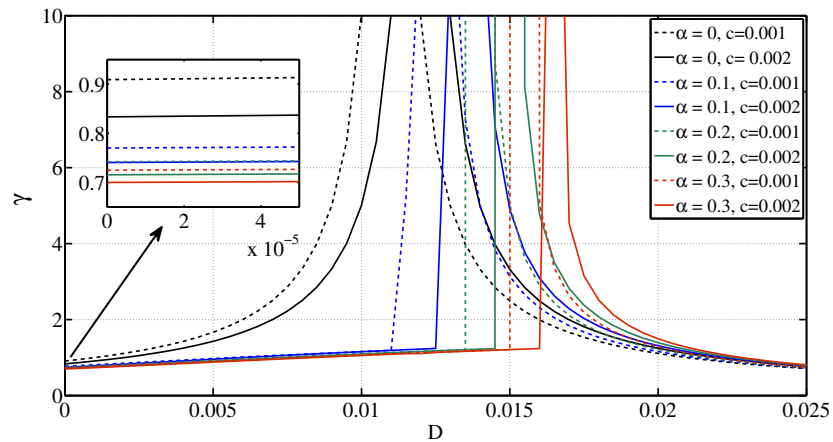

Figure 4.16: Effect of damping on localization vs disorder. Two values of 'c' are chosen. It may be seen that greater damping increases localization for zero disorder.

4.5 Conclusions

In this chapter, the effect of small nonlinearities on a two degree of freedom system has been studied. A case of coupled oscillators - a two mass three spring system, a widely studied model, has been considered. Localization ratio as a function of disorder under harmonic forces and under varying degrees of coupling has been thoroughly investigated for linear and nonlinear domains.

Curve veering in the context of localization has been studied for these two systems and it has been shown that both the phenomena predominantly occur under the case of weak coupling. It has further been shown that mode swapping occurs under weak coupling alone (an indicator of curve veering) and that localization also occurs under similar conditions. It has been shown that localization is mainly a function of disorder and coupling and that it increases with increasing disorder and decreasing coupling for linear behaviour. It has additionally been shown that there are regions of de-localization in the linear domain, which are attributed to singularities.

The effect of nonlinearity on the spring mass system has been considered. It has been assumed that the coupling spring is linear and that there is cubic nonlinearity only in the ground springs. A one-term Harmonic Balance method yields analytical solutions for the nonlinear system. Under the influence of small nonlinearities the following conclusions may be made for the case of weak disorder: (i) hardening nonlinearity aids localization; (ii) softening nonlinearity de-localizes a system; (iii) damping aids localization; and (iv) Increased force amplitudes aids localization. Furthermore, as one increases disorder in the system, the singularities are encountered and the region to the right of the singularity shows exactly the opposite results. However at large disorder values, the localization ratios converge to a linear value, as in these regions, disorder greatly dominates coupling.

The regions of singularities can be exploited for potential use in sensors to detect minute perturbations to the system parameters. It should be remembered that the current analytical approach is limited to small nonlinearities alone such that the system displays periodic response. The influence of large nonlinearities remains to be explored in future studies.

Chapter 5

Conclusions

5.1 Contribution

The main objective for this thesis was to understand spatial localization of dynamic response in periodic structures resulting from different mechanisms. Important findings of this work are summarized below.

1. *Receptance technique* developed in this thesis can be successfully used to predict the location and widths of bandgaps in any periodic system. The following insights were obtained concerning the sub-Bragg bandgaps induced by local resonators.

   - Increasing the mass of the attached resonator increases the width of the bandgap.

   - Increasing the stiffness of the attached resonator also increases the width of the bandgap.

   - In order to maintain the same target frequency of the bandgap (sub-Bragg frequencies), the mass and stiffness have to be increased proportionally.

   - Increasing the damping of the absorber decreases the width of the bandgap as it makes the attached resonator more rigid.

This analysis has useful applications in the design of PC's wherein a careful trade-off needs to be made in order to obtain the best possible width of the bandgap. Additionally, it was found that while periodic masses produce only Bragg bandgaps, attaching local resonators produce only sub-Bragg bandgaps while narrowing down the Bragg bandgaps. The use of two fold periodicity helps in creating a sub-Bragg bandgap while preserving Bragg bandgaps. The Bragg bandgaps could always be tailored accordingly. These results have been proven both analytically using FE methods and experimentally on a structural scale with tests on beams.

2. The second contribution of this work is the experiments performed on a one-dimensional periodic system. We considered a periodic system at a structural scale in the form of a beam with periodic attachments. We measured the responses of the beam to a unit impulse for various types of periodicity and identified the bandgap formation similar to what was observed through FE techniques.

3. The third contribution of this thesis lies in the analysis of two degree of freedom systems. Linear analysis of spring mass systems led to the following observations.

   - Weak coupling and strong disorder promote localization and veering of eigenvalues.
   - The system shows peaks in localization ratio. It is found that for a linear system, the singularity condition is defined as $|\frac{D}{D-C}|$ and therefore it occurs when the disorder is equal to the coupling, if the disorder is additive in the second mass.

4. As nonlinearity is introduced in the system, the following conclusions may be made:

   - For small disorder and given coupling, nonlinearity itself may either localize or delocalize the system, depending on whether the nonlinearity is softening or hardening in nature. Hardening nonlinearity localizes whereas softening nonlinearity de-localizes.

- For large disorder, the opposite is true. Hardening nonlinearity delocalizes whereas softening nonlinearity aids localization.

- Increasing the external force on the system is equivalent to introducing more nonlinearity and therefore contributes to the same effects as those of increasing nonlinearity.

- Damping promotes localization.

5.2   Future Work

1. It is known that nonlinearity may aid in tuning bandgaps further and opportunities to enhance the performance of linear periodic systems. Local resonance analysis has been conducted assuming that the attached resonators are linear. The effect of non-linear local resonators on the sub-Bragg bandgaps makes for an interesting future study. The materials that are being used as soft coatings in PC's are often subjected to large deformities, which introduce material nonlinearities. Thus, the study of the effect of nonlinearities on the bandgaps is important.

2. Experiments included tests on one-dimensional systems. The effect of local resonators on sub-Bragg bandgaps in two and three dimensional systems, especially with the consideration of nonlinearity remains for future work.

3. Localization was studied only for a simple two-degree of freedom model with mild nonlinearity. The effects of strong nonlinearity on multi degree of freedom systems is a vastly debated subject and offers many avenues for research. Similarly, veering was noted for only linear systems in this dissertation. The influence of nonlinearity on veering may further be explored. This may greatly aid in improving sensitivity analysis is micro-mechanical systems.

4. Anderson localization is a statistical phenomenon. A study of nonlinearity with regards to localization with a statistical approach is to be pursued.

5. Finally, the experiments performed in this work need to incorporate the effects of nonlinearity on localization.

Bibliography

[1] H. Huang, C. Sun, and G. Huang, "On the negative effective mass density in acoustic metamaterials," *International Journal of Engineering Science*, vol. 47, no. 4, pp. 610 – 617, 2009. vii, 4, 6

[2] T. A. Schaedler, A. J. Jacobsen, A. Torrents, A. E. Sorensen, J. Lian, J. R. Greer, L. Valdevit, and W. B. Carter, "Ultralight metallic microlattices," *Science*, vol. 334, no. 6058, pp. 962–965, 2011. 1

[3] Z. Liu, X. Zhang, Y. Mao, Y. Y. Zhu, Z. Yang, C. T. Chan, and P. Sheng, "Locally resonant sonic materials," *Science*, vol. 289, pp. 1734–1736, 2000. 1, 3, 4

[4] N. A. Fleck, V. S. Deshpande, and M. F. Ashby, "Micro-architectured materials: past, present and future," *Proceedings of the Royal Society A: Mathematical, Physical and Engineering Science*, vol. 466, no. 2121, pp. 2495–2516, 2010. 1

[5] O. Sigmund and S. Jensen, "Systematic design of phononic bandgap materials and structures by topology optimization," *Philosophical Transactions of the Royal Society of London. Series A: Mathematical, Physical and Engineering Sciences*, vol. 361, no. 1806, pp. 1001–1019, 2003. 1, 2

[6] A. S. Phani, J. Woodhouse, and N. A. Fleck, "Wave propagation in two-dimensional periodic lattices," *The Journal of the Acoustical Society of America*, vol. 119, no. 4, pp. 1995–2005, 2006. 1, 16, 17, 22, 23

[7] M.-H. Lu, L. Feng, and Y.-F. Chen, "Phononic crystals and acoustic metamaterials," *Materials Today*, vol. 12, no. 12, pp. 34 – 42, 2009. 1, 4

[8] J. D. Maynard, "Acoustical analogs of condensed-matter problems," *Rev. Mod. Phys.*, vol. 73, pp. 401–417, May 2001. 1, 11, 58

[9] B. R. Mace, R. W. Jones, and N. R. Harland, "Wave transmission through structural inserts," *The Journal of the Acoustical Society of America*, vol. 109, no. 4, pp. 1417–1421, 2001.

[10] R. Langley, N. Bardell, and H. Ruivo, "The response of two-dimensional periodic structures to harmonic point loading: A theoretical and experimental study of a beam grillage," *Journal of Sound and Vibration*, vol. 207, no. 4, pp. 521 – 535, 1997. 1

[11] P. D. Cha and C. Pierre, "Vibration localization by disorder in assemblies of monocoupled, multimode component systems," *Journal of Applied Mechanics*, vol. 58, no. 4, pp. 1072–1081, 1991. 1, 8

[12] O. O. Bendiksen and N. A. Valero, "Vibration characteristics of mistuned shrouded blade assemblies," *Journal of Engineering for Gas Turbines and Power*, vol. 108, pp. 293–299, 1986. 1, 8

[13] L. Brillouin, *Wave Propagation in Periodic Structures*. Dover Phoenix Editions, Dover Publications, 2003. 2, 16, 17

[14] L. Rayleigh, "On the influence of obstacles arranged in rectangular order upon the properties of a medium," *Philosophical Magazine Series 5*, vol. 34, no. 211, pp. 481–502, 1892. 3

[15] C. Kittel, *Introduction to Solid State Physics, 7th Ed.* Wiley India Pvt. Limited, 2007.

[16] C. H. Hodges and J. Woodhouse, "Vibration isolation from irregularity in a nearly periodic structure: Theory and measurements," *The Journal of the Acoustical Society of America*, vol. 74, no. 3, pp. 894–905, 1983. 7, 8, 9, 10, 58

[17] D. Mead, "Wave propagation and natural modes in periodic systems: I. mono-coupled systems," *Journal of Sound and Vibration*, vol. 40, no. 1, pp. 1 – 18, 1975. 15, 16, 17, 25

[18] D. Mead, "Wave propagation and natural modes in periodic systems: Ii. multi-coupled systems, with and without damping," *Journal of Sound and Vibration*, vol. 40, no. 1, pp. 19 – 39, 1975. 16

[19] D. Mead, "Wave propagation in continuous periodic structures: Research contributions from southampton, 1964âĂŞ1995," *Journal of Sound and Vibration*, vol. 190, no. 3, pp. 495 – 524, 1996. 3, 7, 16, 58

[20] M. S. Kushwaha, P. Halevi, L. Dobrzynski, and B. Djafari-Rouhani, "Acoustic band structure of periodic elastic composites," *Phys. Rev. Lett.*, vol. 71, pp. 2022–2025, Sep 1993. 3

[21] M. Kafesaki, M. Sigalas, and E. Economou, "Elastic wave band gaps in 3-d periodic polymer matrix composites," *Solid State Communications*, vol. 96, pp. 285 – 289, 1995. 3

[22] J.-C. Hsu, "Local resonances-induced low-frequency band gaps in two-dimensional phononic crystal slabs with periodic stepped resonators," *Journal of Physics D: Applied Physics*, vol. 44, 2011. 3, 6

[23] M. S. Kushwaha and B. Djafari-Rouhani, "Giant sonic stop bands in two-dimensional periodic system of fluids," *Journal of Applied Physics*, vol. 84, pp. 4677–4683, 1998. 3

[24] J. V. Sanchez-Perez, C. Rubio, R. Martinez-Sala, R. Sanchez-Grandia, and V. Gomez, "Acoustic barriers based on periodic arrays of scatterers," *Applied Physics Letters*, vol. 81, pp. 5240–5242, 2002. 3

[25] R. L. Weaver and J. Burkhardt, "Weak anderson localization and enhanced backscatter in reverberation rooms and quantum dots," *The Journal of the Acoustical Society of America*, vol. 96, no. 5, pp. 3186–3190, 1994. 3

[26] M. Hirsekorn, "Small-size sonic crystals with strong attenuation bands in the audible frequency range," *Applied Physics Letters*, vol. 84, pp. 3364–3366, 2004. 3, 6

[27] Z. G. Wang, S. H. Lee, C. K. Kim, C. M. Park, K. Nahm, and S. A. Nikitov, "Acoustic wave propagation in one-dimensional phononic crystals containing helmholtz resonators," *Journal of Applied Physics*, vol. 103, p. 064907, 2008. 4, 6

[28] Y. Gu, X. Luo, and H. Ma, "Low frequency elastic wave propagation in two dimensional locally resonant phononic crystal with asymmetric resonator," *Journal of Applied Physics*, vol. 105, no. 4, p. 044903, 2009.

[29] M. Hirsekorn, P. P. Delsanto, A. C. Leung, and P. Matic, "Elastic wave propagation in locally resonant sonic material: Comparison between local interaction simulation approach and modal analysis," *Journal of Applied Physics*, vol. 99, p. 124912, 2006. 34

[30] C. Goffaux, J. Sánchez-Dehesa, and P. Lambin, "Comparison of the sound attenuation efficiency of locally resonant materials and elastic band-gap structures," *Phys. Rev. B*, vol. 70, p. 184302, 2004.

[31] W. Gang, S. Li-Hui, L. Yao-Zong, and W. Ji-Hong, "Accurate evaluation of lowest band gaps in ternary locally resonant phononic crystals," *Chinese Physics*, vol. 15, p. 1843, 2006. 4

[32] D. Yu, Y. Liu, G. Wang, H. Zhao, and J. Qiu, "Flexural vibration band gaps in timoshenko beams with locally resonant structures," *Journal of Applied Physics*, vol. 100, no. 12, p. 124901, 2006. 4

[33] F. R. Montero de Espinosa, E. Jiménez, and M. Torres, "Ultrasonic band gap in a periodic two-dimensional composite," *Phys. Rev. Lett.*, vol. 80, pp. 1208–1211, 1998. 4

[34] L. Liu and M. I. Hussein, "Wave motion in periodic flexural beams and characterization of the transition between bragg scattering and local resonance," *Journal of Applied Mechanics*, vol. 79, p. 011003, 2012. 4, 15

[35] Z. Bo and Z. Li, "New analytical model for composite materials containing local resonance units," *Journal of Engineering Mechanics*, vol. 137, no. 1, pp. 1–7, 2011. 4

[36] H. Sun, X. Du, and P. Pai, "Theory of metamaterial beams for broadband vibration absorption," *Journal of Intelligent Material Systems and Structures*, vol. 21, no. 11, pp. 1085–1101, 2010. 4

[37] J. D. Smith, "Application of the method of asymptotic homogenization to an acoustic metafluid," *Proceedings of the Royal Society A: Mathematical, Physical and Engineering Science*, 2011. 4, 5

[38] K. M. Ho, C. K. Cheng, Z. Yang, X. X. Zhang, and P. Sheng, "Broadband locally resonant sonic shields," *Applied Physics Letters*, vol. 83, pp. 5566–5568, 2003. 6, 15

[39] A. Khelif, A. Choujaa, S. Benchabane, B. Djafari-Rouhani, and V. Laude, "Guiding and bending of acoustic waves in highly confined phononic crystal waveguides," *Applied Physics Letters*, vol. 84, pp. 4400–4402, 2004. 6

[40] Y. Gu, X. Luo, and H. Ma, "Low frequency elastic wave propagation in two dimensional locally resonant phononic crystal with asymmetric resonator," *Journal of Applied Physics*, vol. 105, p. 044903, 2009. 6

[41] E. Fuster-Garcia, V. Romero-Garcia, J. V. Sanchez-Perez, and L. M. Garcia-Raffi, "Targeted band gap creation using mixed sonic crystal arrays including resonators and rigid scatterers," *Applied Physics Letters*, vol. 90, p. 244104, 2007. 6

[42] A. Krynkin, O. Umnova, A. Y. B. Chong, S. Taherzadeh, and K. Attenborough, "Predictions and measurements of sound transmission through a periodic array of elastic shells in air," *The Journal of the Acoustical Society of America*, vol. 128, no. 6, pp. 3496–3506, 2010. 6

[43] Y. Xiao, J. Wen, and X. Wen, "Flexural wave band gaps in locally resonant thin plates with periodically attached springâĂŞmass resonators," *Journal of Physics D: Applied Physics*, vol. 45, no. 19, p. 195401, 2012. 7

[44] D. Yu, J. Wen, H. Zhao, Y. Liu, and X. Wen, "Vibration reduction by using the idea of phononic crystals in a pipe-conveying fluid," *Journal of Sound and Vibration*, vol. 318, no. 1âĂŞ2, pp. 193 – 205, 2008. 7

[45] C. Hodges, "Confinement of vibration by structural irregularity," *Journal of Sound and Vibration*, vol. 82, no. 3, pp. 411 – 424, 1982. 7, 8, 58

[46] P. W. Anderson, "Absence of diffusion in certain random lattices," *Phys. Rev.*, vol. 109, pp. 1492–1505, Mar 1958. 7

[47] C. Dembowski, H.-D. Gräf, R. Hofferbert, H. Rehfeld, A. Richter, and T. Weiland, "Anderson localization in a string of microwave cavities," *Phys. Rev. E*, vol. 60, pp. 3942–3948, Oct 1999. 7

[48] P. Dean and M. D. Bacon, "The nature of vibrational modes in disordered systems," *Proceedings of the Physical Society*, vol. 81, no. 4, p. 642, 1963. 8

[49] P. A. Lee and T. V. Ramakrishnan, "Disordered electronic systems," *Rev. Mod. Phys.*, vol. 57, pp. 287–337, Apr 1985. 8

[50] G. Ottarsson and C. Pierre, "Vibration and wave localization in a nearly periodic beaded string," *The Journal of the Acoustical Society of America*, vol. 101, no. 6, pp. 3430–3442, 1997. 9

[51] A. Tjavaras and M. Triantafyllou, "Non-linear response of two disordered pendula," *Journal of Sound and Vibration*, vol. 190, no. 1, pp. 65 – 76, 1996. 9, 12, 59

[52] C. Pierre, "Mode localization and eigenvalue loci veering phenomena in disordered structures," *Journal of Sound and Vibration*, vol. 126, no. 3, pp. 485 – 502, 1988. 9, 60

[53] G. J. Kissel, "Localization factor for multichannel disordered systems," *Phys. Rev. A*, vol. 44, pp. 1008–1014, Jul 1991. 9

[54] P. Bisegna and G. Caruso, "Dynamics of disordered periodic structures: Homogenized models," 2008. 9

[55] P. Thiruvenkatanathan, J. Woodhouse, J. Yan, and A. Seshia, "Manipulating vibration energy confinement in electrically coupled microelectromechanical resonator arrays," *Microelectromechanical Systems, Journal of*, vol. 20, no. 1, pp. 157 –164, 2011. 9, 60

[56] C. Pierre, "Weak and strong vibration localization in disordered structures: A statistical investigation," *Journal of Sound and Vibration*, vol. 139, no. 1, pp. 111 – 132, 1990. 10

[57] M. Unge and S. StafstrÃűm, "Anderson localization in two-dimensional disordered systems," *Synthetic Metals*, vol. 139, no. 2, pp. 239 – 244, 2003. 10

[58] S. Gonella and M. Ruzzene, "Homogenization and equivalent in-plane properties of two-dimensional periodic lattices," *International Journal of Solids and Structures*, vol. 45, no. 10, pp. 2897 – 2915, 2008. 10

[59] O. Richoux, C. Depollier, and J. Hardy, "Propagation of mechanical waves in a one-dimensional nonlinear disordered lattice," *Phys. Rev. E*, vol. 73, p. 026611, Feb 2006. 11, 58

[60] A. A. Sukhorukov and Y. S. Kivshar, "Nonlinear guided waves and spatial solitons in a periodic layered medium," *J. Opt. Soc. Am. B*, vol. 19, pp. 772–781, Apr 2002. 11

[61] A. Sukhorukov, Y. Kivshar, H. Eisenberg, and Y. Silberberg, "Spatial optical solitons in waveguide arrays," *Quantum Electronics, IEEE Journal of*, vol. 39, pp. 31 – 50, jan 2003. 11

[62] C. E. Bradley, "Time harmonic acoustic bloch wave propagation in periodic waveguides. part i. theory," *The Journal of the Acoustical Society of America*, vol. 96, no. 3, pp. 1844–1853, 1994. 11

[63] C. E. Bradley, "Time harmonic acoustic bloch wave propagation in periodic waveguides. part ii. experiment," *The Journal of the Acoustical Society of America*, vol. 96, no. 3, pp. 1854–1862, 1994.

[64] C. E. Bradley, "Time-harmonic acoustic bloch wave propagation in periodic waveguides. part iii. nonlinear effects," *The Journal of the Acoustical Society of America*, vol. 98, no. 5, pp. 2735–2744, 1995. 11

[65] A. Dick, B. Balachandran, and C. Mote, "Intrinsic localized modes in microresonator arrays and their relationship to nonlinear vibration modes," *Nonlinear Dynamics*, vol. 54, pp. 13–29, 2008. 12

[66] R. S. MacKay and S. Aubry, "Proof of existence of breathers for time-reversible or hamiltonian networks of weakly coupled oscillators," *Nonlinearity*, vol. 7, no. 6, p. 1623, 1994. 12

[67] V. Rothos and A. Vakakis, "Dynamic interactions of traveling waves propagating in a linear chain with an local essentially nonlinear attachment," *Wave Motion*, vol. 46, no. 3, pp. 174 – 188, 2009. 12

[68] Y. Xiao, B. R. Mace, J. Wen, and X. Wen, "Formation and coupling of band gaps in a locally resonant elastic system comprising a string with attached resonators," *Physics Letters A*, vol. 375, pp. 1485–1491, 2011. 13, 15, 27

[69] W. Yong, H. Qibai, Z. Minggang, and L. Zhanxin, "A new approach of vibration isolation analysis of periodic composite structure based on phononic crystal," *International Journal of Mechanics and Materials in Design*, vol. 3, pp. 103–109, 2006. 15

[70] R. E. D. Bishop and D. C. Johnson, *The mechanics of vibration*. Cambridge University Press, 1960. 16, 18, 24, 26, 28

[71] E. Lee and W. Yang, "On waves in composite materials with periodic structure," *SIAM Journal on Applied Mathematics*, vol. 25, no. 3, pp. 492–499, 1973. 17

[72] J. D. Maynard, "Wave propagation in arrays of scatterers tutorial: Part 1," *Acoustics Today*, vol. 4, no. 4, pp. 12–21, 2008. 31

[73] C. Goffaux, J. Sánchez-Dehesa, A. L. Yeyati, P. Lambin, A. Khelif, J. O. Vasseur, and B. Djafari-Rouhani, "Evidence of fano-like interference phenomena in locally resonant materials," *Phys. Rev. Lett.*, vol. 88, p. 225502, May 2002. 34

[74] M. I. Hussein, "Theory of damped bloch waves in elastic media," *Physical Review B*, vol. 80, pp. 212301–1–212301–4, 2009. 38, 40

[75] A. S. Phani and M. I. Hussein, "Analysis of damped bloch waves by rayleigh perturbation method," *The Journal of the Acoustical Society of America, Under Review*, 2012. 40, 41

[76] S. Rao, *Mechanical Vibrations*. Pearson/Prentice Hall, 2004. 54

[77] A. Vakakis, "Non-linear normal modes (nnms) and their applications in vibration theory: An overview," *Mechanical Systems and Signal Processing*, vol. 11, no. 1, pp. 3 – 22, 1997. 59

[78] D. Aronson, G. Ermentrout, and N. Kopell, "Amplitude response of coupled oscillators," *Physica D: Nonlinear Phenomena*, vol. 41, no. 3, pp. 403 – 449, 1990. 59

[79] R. Kuske and T. Erneux, "Bifurcation to localized oscillations," *European Journal of Applied Mathematics*, vol. 8, pp. 389–402, 1997. 59

[80] B. R. Mace and E. Manconi, "Wave motion and dispersion phenomena: Veering, locking and strong coupling effects," *The Journal of the Acoustical Society of America*, vol. 131, no. 2, pp. 1015–1028, 2012. 60

[81] N. Perkins and C. M. Jr., "Comments on curve veering in eigenvalue problems," *Journal of Sound and Vibration*, vol. 106, no. 3, pp. 451 – 463, 1986. 60

[82] P. Chen and J. Ginsberg, "On the relationship between veering of eigenvalue loci and parameter sensitivity of eigenfunctions," *Journal of vibration and acoustics-transactions of the ASME*, vol. 114, pp. 141–148, APR 1992. 60

[83] N. Stephen, "On veering of eigenvalue loci," *Journal of Vibration and Acoustics*, vol. 131, pp. 054501–[5pp], October 2009. 60

[84] X. Liu, "Behavior of derivatives of eigenvalues and eigenvectors in curve veering and mode localization and their relation to close eigenvalues," *Journal of Sound and Vibration*, vol. 256, no. 3, pp. 551 – 564, 2002. 60